

000 001 002 003 004 005 006 007 008 009 010 011 012 013 014 015 016 017 018 019 020 021 022 023 024 025 026 027 028 029 030 031 032 033 034 035 036 037 038 039 040 041 042 043 044 045 046 047 048 049 050 051 052 053 HUMAN-OBJECT INTERACTION VIA AUTOMATICALLY DESIGNED VLM-GUIDED MOTION POLICY

Anonymous authors

Paper under double-blind review

ABSTRACT

Human-object interaction (HOI) synthesis is crucial for applications in animation, simulation, and robotics. However, existing approaches either rely on expensive motion capture data or require manual reward engineering, limiting their scalability and generalizability. In this work, we introduce the first unified physics-based HOI framework that leverages Vision-Language Models (VLMs) to enable long-horizon interactions with diverse object types — including static, dynamic, and articulated objects. We introduce VLM-Guided Relative Movement Dynamics (RMD), a fine-grained spatio-temporal bipartite representation that automatically constructs goal states and reward functions for reinforcement learning. By encoding structured relationships between human and object parts, RMD enables VLMs to generate semantically grounded, interaction-aware motion guidance without manual reward tuning. To support our methodology, we present Interplay, a novel dataset with thousands of long-horizon static and dynamic interaction plans. Extensive experiments demonstrate that our framework outperforms existing methods in synthesizing natural, human-like motions across both simple single-task and complex multi-task scenarios. For more details, please refer to our project webpage: <https://vlm-rmd.github.io/>.

1 INTRODUCTION

Human-Object Interaction (HOI) understanding is fundamental to advancing embodied AI systems in simulation, animation, and robotics. Existing approaches to HOI learning generally fall into two categories. The first paradigm employs motion tracking policies to imitate reference demonstrations (Wang et al., 2023; 2024a; Xu et al., 2025). While these methods can reproduce specific interaction patterns, they face critical limitations: Their heavy reliance on high-quality motion capture data creates scalability bottlenecks, and their strict adherence to reference trajectories inherently restricts their ability to generate novel interactions beyond the training distribution.

The second paradigm adopts a task-centric perspective, developing specialized policies for individual interactions like sitting (Chao et al., 2021; Zhang et al., 2022) or carrying (Xu et al., 2024b; Szot et al., 2021; Deitke et al., 2022; Gao et al., 2024). However, these methods encounter two fundamental challenges. First, they require labor-intensive reward engineering by domain experts — a particularly demanding requirement given the complex dynamics and contact-rich nature of realistic HOI scenarios (Sutton & Barto, 2018). This manual reward design process inherently limits generalizability across interaction types, creating a need for automated objective formulation. Second, constrained by artificially designed, single-objective reward mechanisms, trained policies often overfit to specific behavioral patterns. Producing task-compliant but biomechanically unrealistic motions that violate natural human kinematics.

Recent efforts such as Eureka (Ma et al., 2023) and Grove (Cui et al., 2025) leverage large language models (LLMs) to automatically generate reward function code. However, they rely on iterative search paradigms that are often sample-inefficient and computationally costly. Xiao et al. (2024) advances this line of work by unifying reward design through a “chain-of-contacts” abstraction, which models an interaction as a discrete sequence of contact events. While conceptually elegant, this formulation overlooks the motion dynamics of interactions and lacks the capacity to model whole-body coordination or accommodate dynamic objects. Consequently, it struggles to handle dynamic interactions and often produces jittery, suboptimal behaviors even in static interaction scenarios.

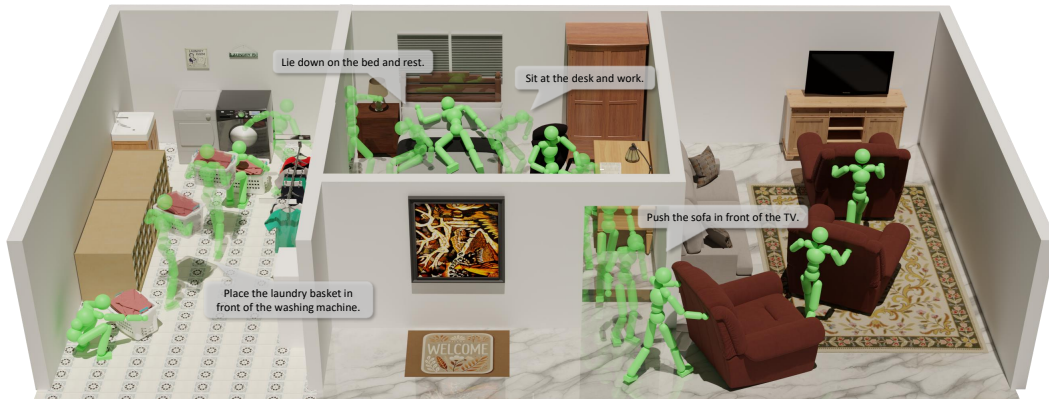


Figure 1: Our framework automatically constructs both goal states and reward functions for diverse interaction tasks in reinforcement learning. By leveraging VLM guidance, the learned motion policy drives physics-based characters to perform coherent, long-horizon interactions with static and dynamic objects, producing natural and task-consistent behaviors.

To address these limitations, we propose a physics-based HOI framework that leverages VLMs to automatically construct goal states and reward functions, guiding the motion policy to perform long-term interactions with diverse objects. Specifically, we aim to empower VLM to provide motion-level, interaction-aware guidance by leveraging its abilities in motion imagination and semantic reasoning. Drawing inspiration from the classical notion of relative motion (Zanstra, 1924), we introduce *Relative Movement Dynamics* (RMD), a structured representation that encodes the fine-grained spatio-temporal relationships between human parts and object parts across an interaction sub-sequence. For example, in the task of lifting a box, the relative spatial configuration between the hands and the box remains stable, providing a natural constraint that captures both discrete interaction goals (e.g., contact) and continuous dynamics (e.g., coordinated movement). RMD is designed to prompt VLMs to imagine interaction dynamics while effectively grounding their high-level reasoning in motion-level patterns. This formulation enables VLMs to move beyond symbolic planning and participate in dynamic skill composition, thereby supporting more expressive and generalizable HOI motion policy learning. Building on RMD, our framework automatically constructs unified goal states that support both static and dynamic interactions, along with automatically designed reward functions that guide motion patterns consistent with the plan.

Our framework supports long-horizon interactions with diverse object types. However, existing datasets typically focus either on static interactions (Xiao et al., 2024) or on object rearrangement (Xu et al., 2024b), and thus fail to cover this setting. To address this gap, we construct a new dataset, *Interplay*, which includes long-horizon static and dynamic interaction tasks across varied scene contexts. This dataset enables systematic evaluation of our framework in a long-horizon, multi-task scenario. Experimental results demonstrate that our method achieves promising quantitative performance and generates natural, human-like motions across a diverse range of HOI tasks.

In summary, our contributions include:

We propose the first unified physics-based HOI synthesis framework for long-horizon human-object interactions leveraging the powerful world knowledge of VLMs, supporting a diverse range of objects, including static, dynamic, and articulated ones.

We introduce VLM-Guided Relative Movement Dynamics (RMD), a fine-grained spatial-temporal bipartite diagram to automatically construct goal states and reward functions for reinforcement learning. This approach bypasses manual reward engineering while supporting diverse HOI, including both static and dynamic interactions.

We introduce *Interplay*, a novel dataset comprising thousands of interaction plans that cover long-horizon static and dynamic interaction tasks. Extensive simulation results demonstrate the effectiveness of our approach on both single-task and long-horizon multi-task scenarios.

108

109

Table 1: Comparative analysis of key features between ours and other methods.

110

111

Methods	Articulated Object	Automated Reward Design	Dynamic Object	Long-horizon Transition	HOI Guidance Granularity	Multitask	High-level Planning	Unified Policy
InterPhys Hassan et al. (2023)			✓		Coarse			
InterScene Pan et al. (2024)				Rule-based FSM	Coarse	✓		✓
TokenHSI Pan et al. (2025)			✓	Rule-based FSM	Coarse	✓		
UniHSI Xiao et al. (2024)				✓	Coarse	✓		
Ours	✓	✓	✓	✓	Fine	✓	✓	✓

112

113

114

115

2 RELATED WORK

116

117

Human Motion Synthesis with Static Scenes. In the field of character animation and motion synthesis, most research has focused on human motion interacting with static 3D scenes (Li et al., 2019; Zhang et al., 2020; Xuan et al., 2023; Zhao et al., 2022; Lee & Joo, 2023; Wang et al., 2022b; 2024b; Starke et al., 2019; Zhao et al., 2023a). Typically, researchers break down complex instructions into several key static poses within the scene (Hassan et al., 2021; Wang et al., 2022a), and then use motion inpainting and optimization techniques to generate transitions between these key poses (Wang et al., 2020). However, this approach often leads to mediocre and inconsistent motions due to the limited expressiveness of the intermediate sequences. Recently, diffusion-based methods like (Ho et al., 2020; Huang et al., 2023; Tang et al., 2024; Yi et al., 2025; Zhao et al., 2024; Tevet et al., 2024) have achieved better results in human-scene synthesis. However, these data-driven approaches are limited to generating short-term motions due to constraints in the dataset, and the physical plausibility of the generated motions is not guaranteed. Apart from data-driven kinematic approaches, some studies have explored the problem within a reinforcement learning framework. For instance, (Zhao et al., 2023b; Zhang & Tang, 2022) achieved long-term goal-oriented behaviors by leveraging motion primitives with specific reward designs. Xiao et al. (2024) decomposes instructions into a sequence of point-reaching control tasks under a unified formulation. However, it addresses only the spatial constraints of static scenes while overlooking the temporal dynamics of objects, rendering it inadequate for managing complex dynamic interactions.

134

135

Kinematic-based Human Motion Synthesis with Dynamic Objects. Research in human motion synthesis has increasingly focused on modeling interactions with dynamic objects (Starke et al., 2020; Jiang et al., 2022; Zhang et al., 2022; 2024). Diffusion-based frameworks (Li et al., 2023b;a; Pi et al., 2023; Peng et al., 2023), guide motion generation with object trajectories but often lack realism due to predefined object paths that fail to account for physical plausibility. In contrast, InterDreamer (Xu et al., 2024a) first generates human motion and subsequently uses a pre-trained world model to produce object trajectories, though this approach is limited by the simplicity of the world model, leading to inaccuracies in trajectory prediction. Some studies attempt to address these limitations by jointly modeling human-object interactions with supplementary guidance techniques, including relation intervention (Wu et al., 2024a), contact prediction (Diller & Dai, 2024), and affordance estimation (Peng et al., 2023). Truman (Jiang et al., 2024b) and Lingo (Jiang et al., 2024a) trained on a high-quality human-scene interaction (HSI) dataset, achieves dynamic stability through an auto-regressive diffusion model guided by action labels or text. Nevertheless, kinematic models continue to face challenges such as penetration, sliding issues, and difficulties in generating long-term motion, requiring extensive annotations.

149

150

151

152

153

154

155

156

157

158

159

160

161

Physics-based Human Motion Synthesis with Dynamic Objects. To generate physically plausible motions, reinforcement learning methods have been shown to effectively train HOI skills using motion capture data (Chao et al., 2021; Merel et al., 2020; Peng et al., 2018; Xie et al., 2023; Xu et al., 2025; Wu et al., 2024b). AMP (Peng et al., 2021) introduced an adversarial motion prior framework for realistic motion synthesis. InterPhys (Hassan et al., 2023) further extended this framework by incorporating an HOI motion prior, achieving success in tasks such as sitting, lying, and carrying. Further advancements have led to successful applications in sports activities, including basketball (Wang et al., 2023; 2024a), tennis (Zhang et al., 2023), skating (Liu & Hodgins, 2017), and soccer (Luo et al., 2024; Liu et al., 2022; Xie et al., 2022). TokenHSI (Pan et al., 2025) integrates multiple skills into a single policy via a task tokenizer. These approaches often depend on heuristic designs and struggle to generalize to longer, multi-round scenarios. Our method seeks to address these limitations by introducing a Relative Movement Dynamics representation, enabling the model to capture both spatial and temporal dynamics effectively. This results in physically plausible and

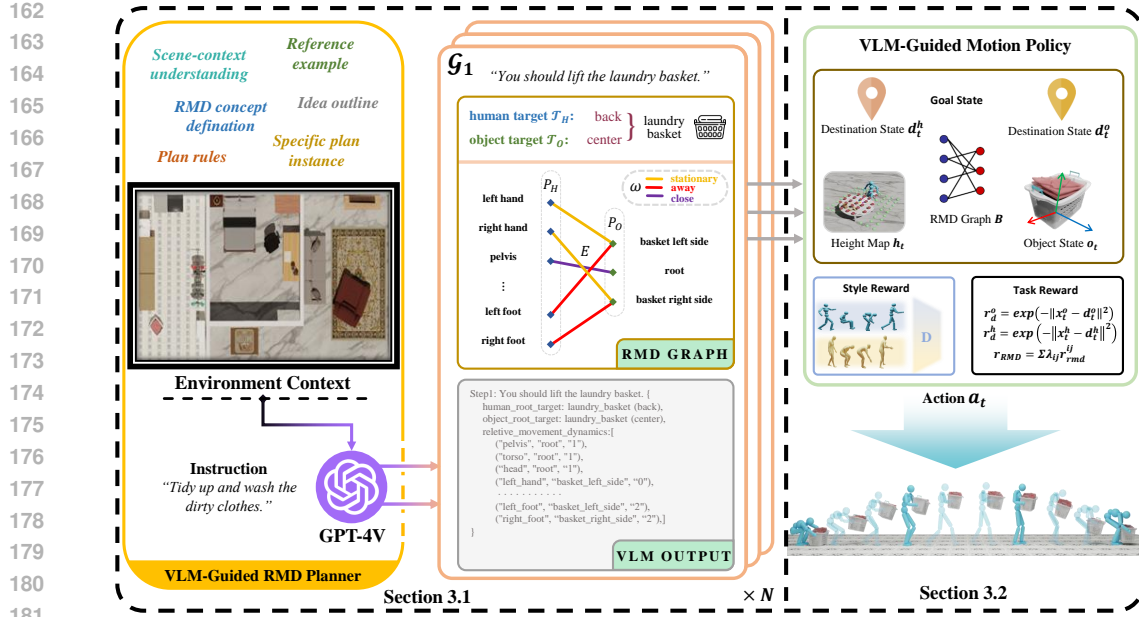


Figure 2: **An overview of our architecture.** Receiving instruction and environment context as input, the VLM-Guided RMD Planner generates a multi-step interaction plan in the form of RMD. Based on this plan, our framework automatically designs both goal states and reward functions, enabling the VLM-Guided Motion Policy to execute the interaction step by step.

temporally coherent interactions, eliminating the need for manual annotations and enhancing realism in dynamic, long-term HOI tasks. The detailed comparisons of key features are listed in Tab. 1.

3 METHOD

Our method comprises two tightly coupled components. First, we describe how a VLM is leveraged to translate high-level instruction and environment context into a sequence of structured interaction plans. This process is grounded in our proposed concept of RMD, which models fine-grained spatio-temporal relationships between human and object parts and serves as the foundation for interaction planning (Sec. 3.1). Then, we present a VLM-guided motion policy learning framework, where each RMD plan is automatically transformed into goal state and a corresponding reward function, enabling the agent to learn executable motion policies without manual specification (Sec. 3.2).

3.1 VLM-GUIDED RMD PLANNER

We employ GPT-4V (Achiam et al., 2023) as our VLM planner to bridge high-level task instructions and low-level interaction execution. As illustrated in Fig. 2, the planner takes three inputs: a high-level textual instruction \mathbf{I} , a top-view contextual image of the environment \mathbf{C} , and a set of modular prompts designed to guide the decomposition of the task into detailed interaction plans.

Effectively leveraging the motion imagination capabilities of VLMs for HOI planning necessitates a principled formulation of the interaction process. Simplistic abstractions, such as the chain-of-contacts (CoC) proposed by UniHSI (Xiao et al., 2024), is inadequate: by imposing only transient point-contact constraints that are discarded immediately upon satisfaction, CoC fails to capture the evolving spatio-temporal relationships critical for modeling dynamic and coordinated interactions. In contrast, we propose a novel concept, *Relative Movement Dynamics* (RMD), which encodes fine-grained spatial and temporal relationships between human body parts and object components throughout the course of an interaction. This structured formulation enables the VLM to reason more effectively about the physical organization of human–object interactions and to produce structured, executable plans aligned with underlying motion dynamics. Our key insight is that human-object interactions can be abstracted as the relative motion between two sets of rigid bodies: human body

216 parts and object parts, evolving over time. We formalize this abstraction as a bipartite graph \mathcal{B} that
 217 encodes part-level motion dynamics. Let
 218

$$P_H = \{p_{h_1}, p_{h_2}, \dots, p_{h_m}\}, \quad P_O = \{p_{o_1}, p_{o_2}, \dots, p_{o_n}\} \quad (1)$$

220 denote the sets of human and object parts, respectively. Then the graph \mathcal{B} is defined as,
 221

$$\mathcal{B} = (V, E, w), \quad V = P_H \cup P_O, \quad E \subseteq P_H \times P_O, \quad w : E \rightarrow \{0, 1, 2, 3\}. \quad (2)$$

223 Each edge $e_{ij} = (p_{h_i}, p_{o_j}) \in E$ connects a human part $p_{h_i} \in P_H$ to an object part $p_{o_j} \in P_O$, with
 224 an associated weight $w_{ij} \in \{0, 1, 2, 3\}$ that characterizes their relative-motion pattern: $w_{ij} = 0$
 225 indicates stationary contact, $w_{ij} = 1$ denotes approaching motion, $w_{ij} = 2$ represents separating
 226 motion, and $w_{ij} = 3$ implies no consistent relative trend.

227 To facilitate the planner’s ability to infer such dynamics, we adopt a modular prompt design strategy.
 228 Each prompt segment is crafted to trigger a specific reasoning ability, such as environmental parsing,
 229 part-level object understanding, motion dynamic inference, or symbolic representation generation.
 230 Through this mechanism, the VLM is guided to produce both the RMD graph \mathcal{B} and two spatial
 231 anchors: the target location for the human root \mathcal{T}_H and the target location for the object root \mathcal{T}_O ,
 232 which together define the global interaction objective.

233 Finally, the planner outputs an interaction plan \mathcal{D} as a sequence of N structured steps,
 234

$$\mathcal{D} = \{\mathcal{G}_1, \mathcal{G}_2, \dots, \mathcal{G}_N\}, \quad (3)$$

236 where each step \mathcal{G}_i is a triplet that specifies the spatial goals and dynamic pattern,
 237

$$\mathcal{G}_i = \{\mathcal{T}_H, \mathcal{T}_O, \mathcal{B}\}. \quad (4)$$

239 3.2 AUTOMATIC POLICY LEARNING VIA VLM-GUIDED RMD

241 Upon receiving the plan generated by the VLM-guided RMD Planner, the policy produces joint-
 242 level torques to actuate the agent and execute the plan. Our physics-based HOI policy learning is
 243 formulated within the framework of goal-conditioned reinforcement learning. At each timestep t ,
 244 the agent samples an action from its policy $\pi(a_t | s_t, g_t)$, conditioned on the current state s_t and the
 245 goal state g_t . After executing the action, the environment transitions to the next state s_{t+1} , and the
 246 agent receives two types of rewards: a task reward $r^G(s_t, g_t, s_{t+1})$, which incentivizes behaviors
 247 aligned with achieving the specified goal g_t , and a style reward $r^S(s_t, s_{t+1})$, which encourages the
 248 agent to produce natural behaviors as proposed in Peng et al. (2021). Unlike AMP and most prior
 249 methods that rely on manually specifying task-specific goal states and handcrafted reward terms, our
 250 framework supports the automatic construction of goal states and reward functions. In the following,
 251 we detail how our framework automatically generates both goal states and reward functions from
 252 VLM output, enabling the agent to learn behaviors aligned with the intended objectives.
 253

254 **Automatic Goal State Construction via VLM-Guided RMD.** To provide the policy with fine-
 255 grained spatio-temporal guidance during the interaction, we encode the i -th planned interaction step
 256 $\mathcal{G}_i = \{\mathcal{T}_H, \mathcal{B}, \mathcal{T}_O\}$, generated by the VLM, with both kinematic and dynamic information.
 257

258 For each edge $e_{ij} \in E$, we extract from the simulator the absolute position–velocity pair of the
 259 human joint, denoted by $\mathbf{p}_{h_i}^p, \mathbf{p}_{h_i}^v$, and that of the nearest surface point on the object part, $\mathbf{p}_{o_j}^p, \mathbf{p}_{o_j}^v$.
 We then compute their relative quantities in the agent-centric coordinate frame,

$$\tilde{\mathbf{p}}_{ij} = \mathbf{p}_{o_j}^p - \mathbf{p}_{h_i}^p, \quad \tilde{\mathbf{v}}_{ij} = \mathbf{p}_{o_j}^v - \mathbf{p}_{h_i}^v. \quad (5)$$

262 The edge weight $w_{ij} \in \{0, 1, 2, 3\}$ is encoded as a one-hot vector $\mathbf{w}'_{ij} \in \{0, 1\}^4$, and concatenated
 263 with the relative position and velocity to form the feature tuple $(\tilde{\mathbf{p}}_{ij}, \tilde{\mathbf{v}}_{ij}, \mathbf{w}'_{ij})$ at timestep t . Stacking
 264 these features across all edges yields the RMD state,
 265

$$\mathbf{s}_t^{\text{RMD}} = \text{concat}_{(i,j) \in E} [\tilde{\mathbf{p}}_{ij}, \tilde{\mathbf{v}}_{ij}, \mathbf{w}'_{ij}] \in \mathbb{R}^{|E| \times (3+3+4)}. \quad (6)$$

266 Both \mathcal{T}_H and \mathcal{T}_O generated by VLM are in the form `object (spatial-relationship)`, e.g.,
 267 `armchair (front)`. For every referenced object we approximate its geometry by an axis-aligned
 268 bounding box with edge lengths l_x, l_y, l_z and center \mathbf{c}_{obj} . We map each spatial-relationship token δ

270 to a displacement vector $\Delta\mathbf{q}(\delta)$ in the object's local frame. For instance, `front` $\mapsto (0.7l_x, 0, 0)$.
 271 The absolute targets for the human root and the object root are defined as,

$$272 \quad \mathbf{p}_{\text{tar}}^h = \mathbf{c}_{\text{obj}} + \Delta\mathbf{q}(\delta_h), \quad \mathbf{p}_{\text{tar}}^o = \mathbf{c}_{\text{obj}} + \Delta\mathbf{q}(\delta_o). \quad (7)$$

274 The destinations proposed by the VLM, originally in the global coordinate system, are transformed
 275 into the agent-centric frame to produce the final destination state,

$$276 \quad \mathbf{d}_t = \{\mathbf{d}_t^h, \mathbf{d}_t^o\}. \quad (8)$$

278 To improve local perception and obstacle avoidance, we attach a fixed-resolution heightmap $\mathbf{h}_t \in$
 279 $\mathbb{R}^{9 \times 9}$ that records the elevation of nearby geometry in the root frame (Tessler et al., 2024; Xiao
 280 et al., 2024). In parallel, we describe object dynamics by the axis-aligned bounding box vertices
 281 $\mathbf{V}_t^{\text{box}} \in \mathbb{R}^{8 \times 3}$, the rotation $\theta_t \in \mathbb{R}^3$, the linear velocity $\mathbf{v}_t \in \mathbb{R}^3$, and the angular velocity $\omega_t \in \mathbb{R}^3$,

$$282 \quad \mathbf{o}_t = \{\mathbf{V}_t^{\text{box}}, \theta_t, \mathbf{v}_t, \omega_t\}. \quad (9)$$

283 By concatenating the RMD state $\mathbf{s}_t^{\text{RMD}}$, the destination \mathbf{d}_t , the heightmap \mathbf{h}_t , and the object state \mathbf{o}_t ,
 284 we construct the complete goal representation,

$$285 \quad \mathbf{g}_t = \{\mathbf{s}_t^{\text{RMD}}, \mathbf{d}_t, \mathbf{h}_t, \mathbf{o}_t\}. \quad (10)$$

287 **Automatic Reward Design via VLM-Guided RMD.** To guide human-object interaction in alignment
 288 with the i -th planned interaction step $\mathcal{G}_i = \{\mathcal{T}_H, \mathcal{B}, \mathcal{T}_O\}$ produced by the VLM, we design a
 289 composite reward function that promotes three key objectives: (i) guiding the human root trajectory
 290 towards the spatial target \mathcal{T}_H , (ii) guiding the object root trajectory towards \mathcal{T}_O , and (iii) enforcing
 291 the relative motion patterns prescribed by the RMD graph \mathcal{B} .

292 To realize these objectives, we define three corresponding reward terms. The term r_d^h encourages
 293 the human root position x_t^h to approach the designated target \mathbf{d}_t^h , and r_d^o encourages the object root
 294 position x_t^o to move toward its designated target \mathbf{d}_t^o ,

$$296 \quad r_d^h = \exp\left(-\|x_t^h - \mathbf{d}_t^h\|^2\right), \quad r_d^o = \exp\left(-\|x_t^o - \mathbf{d}_t^o\|^2\right). \quad (11)$$

298 The term r_{RMD} encourages each edge $e_{ij} \in \mathcal{B}$, representing a (*human-part, object-part*) pair, to
 299 follow the relative motion dynamics specified by its associated edge weight w_{ij} , as planned by the
 300 VLM. Specifically, r_{RMD} is computed by summing the individual alignment reward $r_{\text{rnd}}^{ij}(\cdot)$, each of
 301 which measures how well the pair (p_{h_i}, p_{o_j}) follows the motion pattern defined by w_{ij} , weighted by
 302 a coefficient λ_{ij} ,

$$303 \quad r_{\text{RMD}} = \sum_{(i,j) \in E} \lambda_{ij} \cdot r_{\text{rnd}}(\tilde{\mathbf{p}}_{ij}, \tilde{\mathbf{v}}_{ij}, w_{ij}). \quad (12)$$

305 Further implementation details of $r_{\text{rnd}}^{ij}(\cdot)$ are provided in the appendix. Combining these terms, the
 306 overall task reward at time t is given by,

$$308 \quad r^G(\mathbf{s}_t, \mathbf{g}_t, \mathbf{s}_{t+1}) = \lambda_{\text{RMD}} \cdot r_{\text{RMD}} + \lambda_h \cdot r_d^h + \lambda_o \cdot r_d^o. \quad (13)$$

309 Once the task reward r^G , which is bounded within the range $[0, 1]$, exceeds 0.9, the policy transitions
 310 to the next planned interaction step \mathcal{G}_{i+1} at the following timestep. To balance the contributions of
 311 different reward terms, we adopt adaptive weighting strategies as proposed by Xiao et al. (2024),
 312 which dynamically adjust the value of λ in Eq. 12 and Eq. 13. This design enables the current
 313 reward to be evaluated in a balanced manner and facilitates accurate assessment of progress within
 314 the current stage, thereby ensuring the appropriate timing for transitioning to the next goal.

315 The style reward $r^S(\mathbf{s}_t, \mathbf{s}_{t+1})$ is computed by a discriminator $D(\mathbf{s}_{t-10:t})$ based on a window of
 316 10 consecutive states. Combining the task reward r^G and the style reward r^S , the total reward at
 317 timestep t is defined as,

$$318 \quad r_t = \alpha_{\text{task}} r^G(\mathbf{s}_t, \mathbf{g}_t, \mathbf{s}_{t+1}) + \alpha_{\text{style}} r^S(\mathbf{s}_t, \mathbf{s}_{t+1}). \quad (14)$$

321 4 EXPERIMENT

322 We structure our experiments into two main parts: evaluating HOI skill learning in a complex long-
 323 horizon multi-task scenario (Sec. 4.1) and in a simple single-task scenario (Sec. 4.2).

324

325

Table 2: Comparison with baselines in a long-horizon multi-task scenario.

326

Methods	Completion Rate (%) ↑			Sub-step Completion Ratio (%) ↑			Sub-step Precision (cm) ↓		
	Static Interaction	Dynamic Interaction	Hybrid	Static Interaction	Dynamic Interaction	Hybrid	Static Interaction	Dynamic Interaction	Hybrid
InterPhys [*] Hassan et al. (2023)	21.3	47.8	27.5	37.3	61.9	54.1	13.8	18.7	16.9
TokenHSI [*] Pan et al. (2025)	25.2	52.5	36.0	48.1	65.7	60.1	13.1	16.6	14.4
UniHSI Xiao et al. (2024)	37.2	-	-	61.3	-	-	10.2	-	-
Ours	75.1	71.2	53.8	86.2	84.3	71.8	7.7	13.0	11.2
Ours w/ LLM	62.8	53.1	39.9	81.7	78.3	67.2	8.9	15.2	13.8

331

332

InterPlay Dataset. To evaluate our framework in a long-horizon multi-task scenario, we construct a novel dataset that includes both static and dynamic interaction tasks under diverse scene contexts. We incorporate high-quality 3D object assets from existing datasets, including PartNet (Mo et al., 2019), 3D-FRONT (Fu et al., 2021), SAMP (Hassan et al., 2021), CIRCLE (Araújo et al., 2023), and PartNet-Mobility (Xiang et al., 2020). Each scene contains at least two interactive objects and a minimum of two furniture assets, providing richer contextual complexity for HOI. Further details on dataset construction are provided in the appendix.

333

Implementation Details. To ensure our agent interacts with objects in a natural way, we collect motion clips from SAMP (Hassan et al., 2023), OMOMO (Li et al., 2023a), CIRCLE (Araújo et al., 2023). We conduct experiments in parallel simulated environments within Isaac Gym (Makoviychuk et al., 2021), using PyTorch for neural network implementation. In line with previous studies (Hassan et al., 2023; Xiao et al., 2024), our physical humanoid model consists of 15 rigid body parts and 28 joints, all controlled by a PD controller. We utilize Proximal Policy Optimization (PPO) (Schulman et al., 2017) to train the policy network on an NVIDIA RTX 3090 GPU.

334

335

4.1 EVALUATION IN A LONG-HORIZON MULTI-TASK SCENARIO

336

Real-world applications require agents to perform multiple tasks concurrently or sequentially, requiring advanced coordination and planning. In this context, the agent must interact with multiple objects in sequence according to the plan, which poses significant challenges for ensuring the robustness of VLM-guided motion policy learning and for managing long-horizon transitions.

337

Settings. We split our dataset into three categories: static-interaction, dynamic-interaction, and hybrid setups. In the static-only setup, we sequentially interact with at least two static objects as planned in the dataset. In the dynamic-only setup, we interact with at least two dynamic objects or articulated objects. In the hybrid setup, we select at least three objects, ensuring that at least one dynamic human-object interaction task is included in the overall plan. UniHSI (Xiao et al., 2024) supports only sequential interactions with static objects. We adapt its released prompt to generate plans based on scenarios from our static-only dataset. Both InterPhys (Hassan et al., 2023) and TokenHSI (Pan et al., 2025) support interactions with both static and dynamic objects, but they only cover a subset of HOI tasks. To enable multi-task evaluation, we re-implement their methods by training individual skills in parallel across different environments, manually designing goal states and corresponding reward functions for each. A rule-based finite-state machine is employed to switch between tasks during execution. This adaptation requires substantial manual effort.

338

Metrics. We report the **Completion Rate**, which measures the percentage of trials in which the character sequentially completes all sub-step tasks and returns to a natural standing pose, with the character’s root within 20 cm of the target position. We introduce the **Sub-step Completion Ratio**, which measures the ratio of completed sub-steps to the total number of planned sub-steps. This metric provides a more granular view of the agent’s ability to handle complex tasks with multiple sub-goals. Additionally, we use **Sub-step Precision** to measure the average distance between a specific human part and its target, or between the object root and its target.

339

340

Result Analysis. As shown in Tab. 2, our approach achieves state-of-the-art performance in both individual sub-step execution and long-horizon transitions, reflecting its robustness in handling intricate sequences of actions. Our method benefits from a unified formulation of interaction and fine-grained spatio-temporal guidance for all human body parts, enabling seamless transitions to a multi-task setup. This design not only streamlines the training process by maintaining consistent

378

379

Table 3: Comparison with baselines in a single-task scenario.

Methods	Completion Rate (%) ↑						Success Rate (%) ↑						Precision (cm) ↓					
	Carry	Push	Open	Sit	Lie	Reach	Carry	Push	Open	Sit	Lie	Reach	Carry	Push	Open	Sit	Lie	Reach
AMP* Peng et al. (2021)	53.2	40.4	63.2	7.4	0.9	93.2	74.9	71.0	70.3	77.4	51.9	92.2	17.3	31.7	18.1	13.2	19.1	5.5
InterPhys* Hassan et al. (2023)	67.8	47.1	83.2	23.2	2.7	95.3	88.2	78.1	90.1	88.1	76.4	95.9	12.3	24.7	10.1	10.3	14.8	3.4
TokenHSI* Pan et al. (2025)	71.2	49.3	81.1	27.8	8.9	95.7	92.2	79.5	90.8	92.8	78.2	95.9	11.2	22.5	8.7	9.8	13.2	3.5
UniHSI Xiao et al. (2024)	-	-	-	58.9	23.2	97.1	-	-	-	94.3	81.5	97.5	-	-	-	5.6	12.8	2.1
Ours	88.3	84.1	91.2	92.6	62.0	97.5	93.3	90.1	95.1	95.6	87.0	97.8	10.1	18.2	5.2	4.9	9.1	1.9
multi-one	75.1	71.3	77.9	81.0	49.2	96.2	90.5	86.4	92.1	94.2	83.1	97.2	13.6	21.0	7.3	5.5	14.3	2.0
one-one	11.7	59.2	68.7	65.8	28.1	97.2	14.3	81.2	90.8	92.3	81.6	97.4	21.3	32.2	7.2	9.1	17.2	2.0
w.o. \hat{p}_{ij}	71.7	73.8	77.0	72.9	36.8	96.8	88.9	87.8	90.3	91.8	79.8	96.8	10.9	19.7	10.1	5.6	12.8	2.9
w.o. \hat{v}_{ij}	78.2	76.7	75.2	76.1	42.1	96.9	90.1	84.2	87.8	92.1	79.2	96.9	11.3	20.0	9.9	6.1	14.2	2.5
w.o. \hat{w}_{ij}	69.1	68.4	62.1	67.0	30.3	95.1	82.3	82.3	86.2	90.3	78.9	95.2	14.1	23.9	9.2	7.6	18.6	2.2

384

385

representations across various tasks but also significantly improves the model’s ability to generalize across different interaction scenarios. In the absence of a unified formulation, approaches that naively combine multiple tasks, such as InterPhys and TokenHSI, often encounter difficulties in smoothly switching between tasks. In contrast, our integrated method preserves critical spatial and temporal information throughout the pipeline. While UniHSI excels at approaching and interacting with static objects, it struggles with actions such as getting up after interaction, which notably limits its performance in long-horizon scenarios.

386

387

Ablation. While both VLMs and LLMs possess extensive world knowledge, VLMs exhibit superior spatial awareness and motion imagination thanks to their integration of visual and textual inputs. To evaluate this, we replaced top-view images with textual descriptions and assessed an LLM-based planner under purely textual conditions. The resulting performance drop highlights the essential role of VLMs in our framework. Pretrained on diverse vision-language data, the VLM excels at generating semantically meaningful and spatially grounded plans — capabilities critical for skill learning in complex, multi-object environments. Without VLM guidance, the system struggles to produce coherent long-horizon behaviors, leading to lower task success and degraded motion quality.

405

4.2 EVALUATION IN A SINGLE-TASK SCENARIO

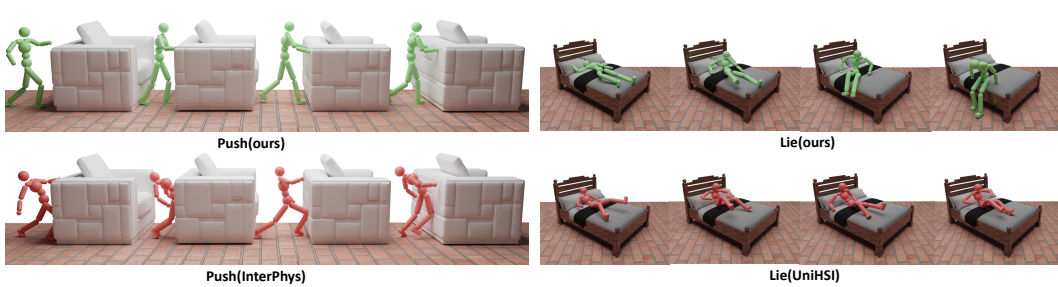
406

Settings. We select a set of interaction tasks from our InterPlay dataset, including both tasks commonly used in prior work and several novel tasks not previously explored. These include three static HOI tasks: reaching, sitting, and lying down, and three dynamic HOI tasks: carrying, pushing, and opening. While previous works (Hassan et al., 2023; Xiao et al., 2024) primarily focus on approaching and interacting with objects, they often overlook a critical aspect: after interacting, the agent must return to a neutral state to facilitate subsequent interactions. For instance, in the sitting task, previous methods consider the task complete once the agent is seated. However, this disregards the need for the agent to return to standing in order to transition smoothly to the next task. Therefore, we redefine the task completion criteria by introducing a “leaving” step: after interacting with an object, the agent must stand up and walk to a designated position. This step ensures that the agent returns to a neutral pose, which is essential for smooth transitions between tasks. For each episode, objects are initialized with a random orientation (ranging from 0 to 2π), a random distance (from 4 to 10 meters), and a random scale (from 0.8 to 1.2). The finish position is then randomly sampled at a point 3 meters away from the object. To ensure a fair comparison with previous state-of-the-art methods, we rigorously followed their established implementation protocols and re-implemented AMP (Peng et al., 2021), InterPhys (Hassan et al., 2023), and TokenHSI (Pan et al., 2025), modifying goal states and reward functions only as necessary to adapt them to our experimental setup.

423

424

Metrics. We first introduce a new metric, **Completion Rate**, to evaluate the percentage of trials in which the character not only completes the interaction with the object but also returns to a neutral standing pose, with the root located within 20 cm of the designated finish position. This metric is designed to reflect the agent’s ability to recover from interaction and complete the full motion sequence, offering a more comprehensive evaluation of control quality. In line with prior works (Hassan et al., 2023; Xiao et al., 2024), we also report the **Success Rate**, which measures the percentage of trials in which the character successfully interacts with the object. A trial is considered successful if the distance between the object’s root and a specific humanoid part is less than 20 cm (for tasks like reaching, sitting, or lying down), or if the distance between the object’s root and



442 **Figure 3: Visualization for qualitative comparison.** Other methods exhibit unnatural motion (In-
 443 terPhys) or incomplete interactions (UniHSI), whereas our method demonstrates human-like motion
 444 quality in qualitative assessments. More qualitative visualization videos can be found in the supple-
 445 mentary materials.

446
 447 the target location is less than 20 cm (for tasks like carrying, pushing, or opening). Furthermore, we
 448 report **Precision** to quantify the average distance between a specific human body part and its cor-
 449 responding target position over the course of the entire interaction in successfully completed trials.
 450 All metrics are evaluated over 4096 trials.

451
 452 **Result Analysis.** As shown in Tab. 3, our method achieves higher or comparable performance
 453 across all these metrics compared to the baselines. Our method outperforms tasks involving the
 454 recovery process of static human-object interactions, such as getting up after sitting or lying down, as
 455 the Relative Movement Dynamics guides each body part to move away from the object. In contrast,
 456 as shown in Fig. 3, UniHSI (Xiao et al., 2024) struggles to get up because it treats the human-object
 457 interaction as a sequence of independent spatial reaching tasks, neglecting the temporal dynamics
 458 that coordinate the movements of different body parts. Similarly, InterPhys (Hassan et al., 2023)
 459 produces unnatural and unstable motions to complete tasks, such as abrupt kicking or thrusting
 460 forward, due to its lack of fine-grained spatio-temporal guidance for coordinating the movements of
 461 different body parts. Instead, our design ensures that the agent keeps both hands and arms relatively
 462 stationary against the back of the sofa.

463
 464 **Ablation.** We conduct an ablation study on key components to evaluate the contribution of the pro-
 465 posed VLM-guided RMD. In the multi-one setup, we simplify object representation by removing the
 466 division into distinct parts and treating the object as a single entity. Representing the object only by
 467 its root pose and kinematic data leads to a slight performance drop, as the model loses fine-grained
 468 geometric information necessary for accurate interaction modeling. In the one-one setup, we restrict
 469 the VLM-guided RMD Planner to model only the dynamics of a single human part interacting with
 470 one object part per sub-step. This disrupts whole-body coordination and often traps optimization in
 471 local optima, resulting in a noticeable decline in performance. These results highlight the effective-
 472 ness of the multi-multi formulation in handling complex interactions. Moreover, removing either
 473 kinematic relation encoding ($\hat{p}_t^{ij}, \hat{v}_t^{ij}$) or dynamic encoding (w_t^{ij}) further degrades performance, as
 474 both are crucial for capturing the spatio-temporal relationships between human and object. Overall,
 475 the ablation results confirm the central role of VLM-guided RMD in our framework.

476 5 CONCLUSION

477
 478 In this paper, we present a physics-based framework for synthesizing diverse Human-Object Inter-
 479 actions, guided by VLMs, through our proposed Relative Movement Dynamics — a spatio-temporal
 480 representation that structures part-level relationships between human and object. RMD automates
 481 the generation of goal states and reward functions for reinforcement learning, eliminating man-
 482 ual engineering while supporting static, dynamic, and articulated interactions. Our method bridges
 483 high-level semantic reasoning with low-level physics-based control, producing natural motions that
 484 outperform task-specific and LLM-based baselines in realism and adaptability. To facilitate evalua-
 485 tion, we introduce the Interplay dataset for long-horizon HOI tasks. Extensive results demonstrate
 the effectiveness of our approach on both single-task and long-horizon multi-task scenarios.

486 REFERENCES
487

488 Josh Achiam, Steven Adler, Sandhini Agarwal, Lama Ahmad, Ilge Akkaya, Florencia Leoni Ale-
489 man, Diogo Almeida, Janko Altenschmidt, Sam Altman, Shyamal Anadkat, et al. Gpt-4 technical
490 report. *arXiv preprint arXiv:2303.08774*, 2023.

491 Joao Pedro Araújo, Jiaman Li, Karthik Vetrivel, Rishi Agarwal, Jiajun Wu, Deepak Gopinath,
492 Alexander William Clegg, and Karen Liu. Circle: Capture in rich contextual environments.
493 In *Proceedings of the IEEE/CVF Conference on Computer Vision and Pattern Recognition*, pp.
494 21211–21221, 2023.

495 Yu-Wei Chao, Jimei Yang, Weifeng Chen, and Jia Deng. Learning to sit: Synthesizing human-
496 chair interactions via hierarchical control. In *Proceedings of the AAAI Conference on Artificial
497 Intelligence*, volume 35, pp. 5887–5895, 2021.

498 Jieming Cui, Tengyu Liu, Ziyu Meng, Jiale Yu, Ran Song, Wei Zhang, Yixin Zhu, and Siyuan
499 Huang. Grove: A generalized reward for learning open-vocabulary physical skill. In *CVPR*,
500 2025.

501 Matt Deitke, Eli VanderBilt, Alvaro Herrasti, Luca Weihs, Kiana Ehsani, Jordi Salvador, Winson
502 Han, Eric Kolve, Aniruddha Kembhavi, and Roozbeh Mottaghi. Procthor: Large-scale embodied
503 ai using procedural generation. *Advances in Neural Information Processing Systems*, 35:5982–
504 5994, 2022.

505 Christian Diller and Angela Dai. Cg-hoi: Contact-guided 3d human-object interaction generation.
506 In *Proceedings of the IEEE/CVF Conference on Computer Vision and Pattern Recognition*, pp.
507 19888–19901, 2024.

508 Huan Fu, Bowen Cai, Lin Gao, Ling-Xiao Zhang, Jiaming Wang, Cao Li, Qixun Zeng, Chengyue
509 Sun, Rongfei Jia, Binqiang Zhao, et al. 3d-front: 3d furnished rooms with layouts and seman-
510 tics. In *Proceedings of the IEEE/CVF International Conference on Computer Vision*, pp. 10933–
511 10942, 2021.

512 Jiawei Gao, Ziqin Wang, Zeqi Xiao, Jingbo Wang, Tai Wang, Jinkun Cao, Xiaolin Hu, Si Liu,
513 Jifeng Dai, and Jiangmiao Pang. Coohoi: Learning cooperative human-object interaction with
514 manipulated object dynamics. *arXiv preprint arXiv:2406.14558*, 2024.

515 Mohamed Hassan, Duygu Ceylan, Ruben Villegas, Jun Saito, Jimei Yang, Yi Zhou, and Michael J
516 Black. Stochastic scene-aware motion prediction. In *Proceedings of the IEEE/CVF International
517 Conference on Computer Vision*, pp. 11374–11384, 2021.

518 Mohamed Hassan, Yunrong Guo, Tingwu Wang, Michael Black, Sanja Fidler, and Xue Bin Peng.
519 Synthesizing physical character-scene interactions. In *ACM SIGGRAPH 2023 Conference Pro-
520 ceedings*, pp. 1–9, 2023.

521 Jonathan Ho, Ajay Jain, and Pieter Abbeel. Denoising diffusion probabilistic models. *Advances in
522 neural information processing systems*, 33:6840–6851, 2020.

523 Siyuan Huang, Zan Wang, Puhao Li, Baoxiong Jia, Tengyu Liu, Yixin Zhu, Wei Liang, and Song-
524 Chun Zhu. Diffusion-based generation, optimization, and planning in 3d scenes. In *Proceedings
525 of the IEEE/CVF Conference on Computer Vision and Pattern Recognition*, pp. 16750–16761,
526 2023.

527 Nan Jiang, Tengyu Liu, Zhexuan Cao, Jieming Cui, Yixin Chen, He Wang, Yixin Zhu, and
528 Siyuan Huang. Chairs: Towards full-body articulated human-object interaction. *arXiv preprint
529 arXiv:2212.10621*, 3, 2022.

530 Nan Jiang, Zimo He, Zi Wang, Hongjie Li, Yixin Chen, Siyuan Huang, and Yixin Zhu. Autonomous
531 character-scene interaction synthesis from text instruction. In *SIGGRAPH Asia 2024 Conference
532 Papers*, pp. 1–11, 2024a.

533 Nan Jiang, Zhiyuan Zhang, Hongjie Li, Xiaoxuan Ma, Zan Wang, Yixin Chen, Tengyu Liu, Yixin
534 Zhu, and Siyuan Huang. Scaling up dynamic human-scene interaction modeling. In *Proceed-
535 ings of the IEEE/CVF Conference on Computer Vision and Pattern Recognition*, pp. 1737–1747,
536 2024b.

540 Jiye Lee and Hanbyul Joo. Locomotion-action-manipulation: Synthesizing human-scene interactions in complex 3d environments. In *Proceedings of the IEEE/CVF International Conference on Computer Vision (ICCV)*, 2023.

541

542

543

544 Jiaman Li, Alexander Clegg, Roozbeh Mottaghi, Jiajun Wu, Xavier Puig, and C Karen Liu. Controllable human-object interaction synthesis. *arXiv preprint arXiv:2312.03913*, 2023a.

545

546 Jiaman Li, Jiajun Wu, and C Karen Liu. Object motion guided human motion synthesis. *ACM Transactions on Graphics (TOG)*, 42(6):1–11, 2023b.

547

548

549 Xuetong Li, Sifei Liu, Kihwan Kim, Xiaolong Wang, Ming-Hsuan Yang, and Jan Kautz. Putting humans in a scene: Learning affordance in 3d indoor environments. In *Proceedings of the IEEE/CVF conference on computer vision and pattern recognition*, pp. 12368–12376, 2019.

550

551

552

553 Libin Liu and Jessica Hodgins. Learning to schedule control fragments for physics-based characters using deep q-learning. *ACM Transactions on Graphics (TOG)*, 36(3):1–14, 2017.

554

555 Siqi Liu, Guy Lever, Zhe Wang, Josh Merel, SM Ali Eslami, Daniel Hennes, Wojciech M Czarnecki, Yuval Tassa, Shayegan Omidshafiei, Abbas Abdolmaleki, et al. From motor control to team play in simulated humanoid football. *Science Robotics*, 7(69):eab0235, 2022.

556

557

558

559 Zhengyi Luo, Jiashun Wang, Kangni Liu, Haotian Zhang, Chen Tessler, Jingbo Wang, Ye Yuan, Jinkun Cao, Zihui Lin, Fengyi Wang, et al. Smplolympics: Sports environments for physically simulated humanoids. *arXiv preprint arXiv:2407.00187*, 2024.

560

561

562 Yecheng Jason Ma, William Liang, Guanzhi Wang, De-An Huang, Osbert Bastani, Dinesh Jayaraman, Yuke Zhu, Linxi Fan, and Anima Anandkumar. Eureka: Human-level reward design via coding large language models. *arXiv preprint arXiv: Arxiv-2310.12931*, 2023.

563

564

565

566 Viktor Makoviychuk, Lukasz Wawrzyniak, Yunrong Guo, Michelle Lu, Kier Storey, Miles Macklin, David Hoeller, Nikita Rudin, Arthur Allshire, Ankur Handa, et al. Isaac gym: High performance gpu-based physics simulation for robot learning. *arXiv preprint arXiv:2108.10470*, 2021.

567

568

569

570 Josh Merel, Saran Tunyasuvunakool, Arun Ahuja, Yuval Tassa, Leonard Hasenclever, Vu Pham, Tom Erez, Greg Wayne, and Nicolas Heess. Catch & carry: reusable neural controllers for vision-guided whole-body tasks. *ACM Transactions on Graphics (TOG)*, 39(4):39–1, 2020.

571

572

573 Kaichun Mo, Shilin Zhu, Angel X. Chang, Li Yi, Subarna Tripathi, Leonidas J. Guibas, and Hao Su. PartNet: A large-scale benchmark for fine-grained and hierarchical part-level 3D object understanding. In *The IEEE Conference on Computer Vision and Pattern Recognition (CVPR)*, June 2019.

574

575

576

577

578 Liang Pan, Jingbo Wang, Buzhen Huang, Junyu Zhang, Haofan Wang, Xu Tang, and Yangang Wang. Synthesizing physically plausible human motions in 3d scenes. In *2024 International Conference on 3D Vision (3DV)*, pp. 1498–1507. IEEE, 2024.

579

580

581 Liang Pan, Zeshi Yang, Zhiyang Dou, Wenjia Wang, Buzhen Huang, Bo Dai, Taku Komura, and Jingbo Wang. Tokenhs: Unified synthesis of physical human-scene interactions through task tokenization. In *CVPR*, 2025.

582

583

584

585 Xiaogang Peng, Yiming Xie, Zizhao Wu, Varun Jampani, Deqing Sun, and Huaizu Jiang. Hoi-diff: Text-driven synthesis of 3d human-object interactions using diffusion models. *arXiv preprint arXiv:2312.06553*, 2023.

586

587

588 Xue Bin Peng, Pieter Abbeel, Sergey Levine, and Michiel Van de Panne. Deepmimic: Example-guided deep reinforcement learning of physics-based character skills. *ACM Transactions On Graphics (TOG)*, 37(4):1–14, 2018.

589

590

591 Xue Bin Peng, Ze Ma, Pieter Abbeel, Sergey Levine, and Angjoo Kanazawa. Amp: Adversarial motion priors for stylized physics-based character control. *ACM Transactions on Graphics (ToG)*, 40(4):1–20, 2021.

592

593

594 Huaijin Pi, Sida Peng, Minghui Yang, Xiaowei Zhou, and Hujun Bao. Hierarchical generation of
 595 human-object interactions with diffusion probabilistic models. In *Proceedings of the IEEE/CVF*
 596 *International Conference on Computer Vision*, pp. 15061–15073, 2023.

597

598 John Schulman, Filip Wolski, Prafulla Dhariwal, Alec Radford, and Oleg Klimov. Proximal policy
 599 optimization algorithms. *arXiv preprint arXiv:1707.06347*, 2017.

600

601 Sebastian Starke, He Zhang, Taku Komura, and Jun Saito. Neural state machine for character-scene
 602 interactions. *ACM Transactions on Graphics*, 38(6):178, 2019.

603

604 Sebastian Starke, Yiwei Zhao, Taku Komura, and Kazi Zaman. Local motion phases for learning
 605 multi-contact character movements. *ACM Transactions on Graphics (TOG)*, 39(4):54–1, 2020.

606

607 Richard S. Sutton and Andrew G. Barto. *Reinforcement Learning: An Introduction*. A Bradford
 608 Book, Cambridge, MA, USA, 2018. ISBN 0262039249.

609

610 Andrew Szot, Alexander Clegg, Eric Undersander, Erik Wijmans, Yili Zhao, John Turner, Noah
 611 Maestre, Mustafa Mukadam, Devendra Singh Chaplot, Oleksandr Maksymets, et al. Habitat 2.0:
 612 Training home assistants to rearrange their habitat. *Advances in neural information processing*
 613 systems, 34:251–266, 2021.

614

615 Jiangnan Tang, Jingya Wang, Kaiyang Ji, Lan Xu, Jingyi Yu, and Ye Shi. A unified diffusion
 616 framework for scene-aware human motion estimation from sparse signals. In *Proceedings of the*
 617 *IEEE/CVF Conference on Computer Vision and Pattern Recognition*, pp. 21251–21262, 2024.

618

619 Chen Tessler, Yunrong Guo, Ofir Nabati, Gal Chechik, and Xue Bin Peng. Maskedmimic: Uni-
 620 fied physics-based character control through masked motion inpainting. *ACM Transactions on*
 621 *Graphics (TOG)*, 2024.

622

623 Guy Tevet, Sigal Raab, Setareh Cohan, Daniele Reda, Zhengyi Luo, Xue Bin Peng, Amit H
 624 Bermano, and Michiel van de Panne. Closd: Closing the loop between simulation and diffu-
 625 sion for multi-task character control. *arXiv preprint arXiv:2410.03441*, 2024.

626

627 Jiajun Wang, Huazhe Xu, Jingwei Xu, Sifei Liu, and Xiaolong Wang. Synthesizing long-term 3d
 628 human motion and interaction in 3d scenes, 2020.

629

630 Jingbo Wang, Yu Rong, Jingyuan Liu, Sijie Yan, Dahua Lin, and Bo Dai. Towards diverse and
 631 natural scene-aware 3d human motion synthesis. In *Proceedings of the IEEE/CVF Conference on*
 632 *Computer Vision and Pattern Recognition*, pp. 20460–20469, 2022a.

633

634 Yinhuai Wang, Jing Lin, Ailing Zeng, Zhengyi Luo, Jian Zhang, and Lei Zhang. Physhoi: Physics-
 635 based imitation of dynamic human-object interaction. *arXiv preprint arXiv:2312.04393*, 2023.

636

637 Yinhuai Wang, Qihan Zhao, Runyi Yu, Ailing Zeng, Jing Lin, Zhengyi Luo, Hok Wai Tsui, Jiwen
 638 Yu, Xiu Li, Qifeng Chen, Jian Zhang, Lei Zhang, and Tan Ping. Skillmimic: Learning reusable
 639 basketball skills from demonstrations. *arXiv preprint arXiv:2408.15270*, 2024a.

640

641 Zan Wang, Yixin Chen, Tengyu Liu, Yixin Zhu, Wei Liang, and Siyuan Huang. Humanise:
 642 Language-conditioned human motion generation in 3d scenes. *Advances in Neural Information*
 643 *Processing Systems*, 35:14959–14971, 2022b.

644

645 Zan Wang, Yixin Chen, Baoxiong Jia, Puhao Li, Jinlu Zhang, Jingze Zhang, Tengyu Liu, Yixin
 646 Zhu, Wei Liang, and Siyuan Huang. Move as you say, interact as you can: Language-guided
 647 human motion generation with scene affordance. In *Proceedings of the IEEE/CVF Conference on*
 648 *Computer Vision and Pattern Recognition (CVPR)*, 2024b.

649

650 Qianyang Wu, Ye Shi, Xiaoshui Huang, Jingyi Yu, Lan Xu, and Jingya Wang. Thor: Text to human-
 651 object interaction diffusion via relation intervention. *arXiv preprint arXiv:2403.11208*, 2024a.

652

653 Zhen Wu, Jiaman Li, Pei Xu, and C. Karen Liu. Human-object interaction from human-level in-
 654 structions, 2024b. URL <https://arxiv.org/abs/2406.17840>.

648 Fanbo Xiang, Yuzhe Qin, Kaichun Mo, Yikuan Xia, Hao Zhu, Fangchen Liu, Minghua Liu, Hanxiao
 649 Jiang, Yifu Yuan, He Wang, Li Yi, Angel X. Chang, Leonidas J. Guibas, and Hao Su. SAPIEN: A
 650 simulated part-based interactive environment. In *The IEEE Conference on Computer Vision and*
 651 *Pattern Recognition (CVPR)*, June 2020.

652 Zeqi Xiao, Tai Wang, Jingbo Wang, Jinkun Cao, Wenwei Zhang, Bo Dai, Dahua Lin, and Jiang-
 653 miao Pang. Unified human-scene interaction via prompted chain-of-contacts. In *The Twelfth*
 654 *International Conference on Learning Representations*, 2024.

655 Zhaoming Xie, Sebastian Starke, Hung Yu Ling, and Michiel van de Panne. Learning soccer juggling
 656 skills with layer-wise mixture-of-experts. In *ACM SIGGRAPH 2022 Conference Proceedings*, pp.
 657 1–9, 2022.

658 Zhaoming Xie, Jonathan Tseng, Sebastian Starke, Michiel van de Panne, and C Karen Liu. Hier-
 659 archical planning and control for box loco-manipulation. *Proceedings of the ACM on Computer*
 660 *Graphics and Interactive Techniques*, 6(3):1–18, 2023.

661 Sirui Xu, Ziyin Wang, Yu-Xiong Wang, and Liang-Yan Gui. Interdreamer: Zero-shot text to 3d
 662 dynamic human-object interaction. *arXiv preprint arXiv:2403.19652*, 2024a.

663 Sirui Xu, Hung Yu Ling, Yu-Xiong Wang, and Liangyan Gui. Intermimic: Towards universal whole-
 664 body control for physics-based human-object interactions. In *CVPR*, 2025.

665 Xinyu Xu, Yizheng Zhang, Yong-Lu Li, Lei Han, and Cewu Lu. Humanvla: Towards vision-
 666 language directed object rearrangement by physical humanoid. *arXiv preprint arXiv:2406.19972*,
 667 2024b.

668 Haibiao Xuan, Xiongzheng Li, Jinsong Zhang, Hongwen Zhang, Yebin Liu, and Kun Li. Narrator:
 669 Towards natural control of human-scene interaction generation via relationship reasoning. In
 670 *Proceedings of the IEEE/CVF International Conference on Computer Vision (ICCV)*, pp. 22268–
 22278, October 2023.

671 Hongwei Yi, Justus Thies, Michael J Black, Xue Bin Peng, and Davis Rempe. Generating human
 672 interaction motions in scenes with text control. In *European Conference on Computer Vision*, pp.
 673 246–263. Springer, 2025.

674 Herman Zanstra. A study of relative motion in connection with classical mechanics. *Physical*
 675 *Review*, 23(4):528, 1924.

676 Chengwen Zhang, Yun Liu, Ruofan Xing, Bingda Tang, and Li Yi. Core4d: A 4d human-
 677 object-human interaction dataset for collaborative object rearrangement. *arXiv preprint*
 678 *arXiv:2406.19353*, 2024.

679 Haotian Zhang, Ye Yuan, Viktor Makoviychuk, Yunrong Guo, Sanja Fidler, Xue Bin Peng, and
 680 Kayvon Fatahalian. Learning physically simulated tennis skills from broadcast videos. *ACM*
 681 *Transactions on Graphics (TOG)*, 42(4):1–14, 2023.

682 Siwei Zhang, Yan Zhang, Qianli Ma, Michael J Black, and Siyu Tang. Generating person-scene
 683 interactions in 3d scenes. In *International Conference on 3D Vision (3DV)*, volume 2, 2020.

684 Xiaohan Zhang, Bharat Lal Bhatnagar, Sebastian Starke, Vladimir Guzov, and Gerard Pons-Moll.
 685 Couch: Towards controllable human-chair interactions. In *European Conference on Computer*
 686 *Vision*, pp. 518–535. Springer, 2022.

687 Yan Zhang and Siyu Tang. The wanderings of odysseus in 3d scenes. In *Proceedings of the*
 688 *IEEE/CVF Conference on Computer Vision and Pattern Recognition*, pp. 20481–20491, 2022.

689 Kaifeng Zhao, Shaofei Wang, Yan Zhang, Thabo Beeler, and Siyu Tang. Compositional human-
 690 scene interaction synthesis with semantic control. In *European conference on computer vision*
 691 (*ECCV*), 2022.

692 Kaifeng Zhao, Yan Zhang, Shaofei Wang, Thabo Beeler, and Siyu Tang. DIMOS: Synthesizing
 693 diverse human motions in 3d indoor scenes. In *International conference on computer vision*
 694 (*ICCV*), 2023a.

702 Kaifeng Zhao, Yan Zhang, Shaofei Wang, Thabo Beeler, and Siyu Tang. Synthesizing diverse
703 human motions in 3d indoor scenes. In *Proceedings of the IEEE/CVF International Conference*
704 *on Computer Vision*, pp. 14738–14749, 2023b.

705 Kaifeng Zhao, Gen Li, and Siyu Tang. Dart: A diffusion-based autoregressive motion model for
706 real-time text-driven motion control. *arXiv preprint arXiv:2410.05260*, 2024.

708
709
710
711
712
713
714
715
716
717
718
719
720
721
722
723
724
725
726
727
728
729
730
731
732
733
734
735
736
737
738
739
740
741
742
743
744
745
746
747
748
749
750
751
752
753
754
755

756	APPENDICES	
757		
758	A Details of VLM Planner	15
759		
760	B InterPlay Dataset	18
761		
762	C Additional Details of Reinforcement Learning	18
763		
764	D Visualizations in Supplementary Material	25
765		
766	E Ablation study on the VLM Planner	25
767		
768	F User Study	26
769		
770	G Limitations and Future Work	26
771		
772	H Statements	27
773		
774		
775		
776		

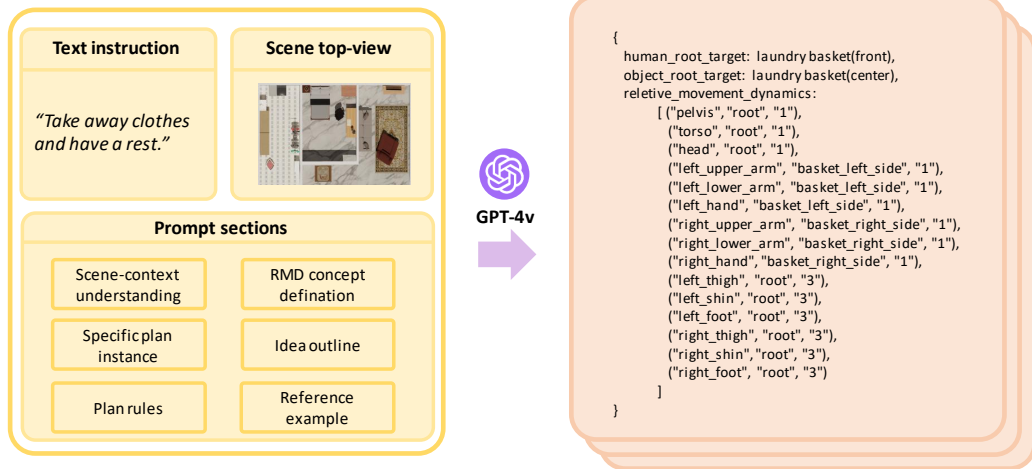


Figure 4: An overview of VLM-guided RMD Planner pipeline.

A DETAILS OF VLM PLANNER

As shown in Fig. 4, given a top-view image of the surrounding scene and a textual instruction, the VLM-guided RMD Planner generates a sequence of sub-step plans in the form of structured JSON. This output format facilitates direct downstream processing via Python scripts.

To ensure that the planner performs as intended, we design prompts that explicitly guide it to understand the concept of Relative Movement Dynamics (RMD), perceive the contextual scene information, decompose high-level instructions, and produce outputs in a structured format consistent with our framework. For clarity and modularity, we organize the prompt into distinct sections, each fulfilling a specific functional role as illustrated in Fig. 5 and Fig. 6. The content of each section is detailed below.

Scene-context Understanding. This section of the prompt helps the planner interpret the scene context and determine the target destination using a simplified relative spatial relationship. Specifically, we reduce spatial relations to seven canonical types: *center*, *forward*, *back*, *left*, *right*, *up*, and *down*.

810

811

812

Prompt section1: scene-context understanding

813

814

815

816

817

818

819

820

821

822

823

824

825

826

827

828

829

830

831

832

833

To effectively plan sequential interactions between humanoid and objects within a scene, it is essential to recognize the type of each object, understand the spatial relationships among them, and identify the most suitable object for interaction at each sub-step, based on the scene's top-down view. We simplify the spatial relationships between objects into seven types: center, forward, back, left, right, up, and down. For example, you can use the term "box (front)" to describe the position that lies in front of the box.

Prompt section3: specific plan instance

```

human_root_target: box(front),
object_root_target: box(center),
relative_movement_dynamics:
[
    ("pelvis", "root", "1"),
    ("torso", "root", ""),
    ("head", "root", "1"),
    ("left_upper_arm", "box_left_side", "0"),
    ("left_lower_arm", "box_left_side", "0"),
    ("left_hand", "box_left_side", "0"),
    ("right_upper_arm", "box_right_side", "0"),
    ("right_lower_arm", "box_right_side", "0"),
    ("right_hand", "box_right_side", "0"),
    ("left_thigh", "root", "3"),
    ("left_shin", "box_left_side", "2"),
    ("left_foot", "box_left_side", "2"),
    ("right_thigh", "root", "3"),
    ("right_shin", "box_right_side", "2"),
    ("right_foot", "box_right_side", "2")
]
}

This instance describes the relative movement dynamics during a scenario where a humanoid bends down to grab a box with both hands and picks it up.

- The "pelvis", "torso", and "head" have an edge weight of 1 with "root" because the distance between the pelvis, torso, head and the box center decreases as the box is gradually lifted.

- The "left_upper_arm", "left_lower_arm", and "left_hand" have an edge weight of 0 with "box_left_side", indicating that these body parts remain relatively stationary with respect to the box side during this time.

- The "left_shin", "left_foot" and "box_left_side" have an edge weight of 3 as the box is leaving with lower part of body.

- The rest of the weight can be obtained in the same way.

- The humanoid does not need to move during interaction, therefore the human_root_target correspond to the position in the front of the box.

- The object does not need to be moved in xy plane during the interaction, therefore the object_root_target corresponds to the position at the center of the box.

```

Prompt section4: idea outline

834

835

836

837

838

839

840

841

842

843

844

845

846

847

848

849

850

851

852

853

854

855

856

857

858

859

860

861

862

863

Prompt section2: RMD concept definition

The **Relative Movement Dynamics** represents the relative movement trend between each human body part and the corresponding object part over a period of time. This trend is modeled as a bipartite graph, where one subset of nodes represents human body parts, and the other subset represents parts of an object.

The subset representing human body parts consists of fifteen nodes corresponding to specific regions of the body:

- pelvis	- torso	- head
- right_upper_arm	- right_lower_arm	- right_hand
- left_upper_arm	- left_lower_arm	- left_hand
- right_thigh	- right_shin	- right_foot
- left_thigh	- left_shin	- left_foot

The subset representing the object parts contains x nodes, where x depends on the specific object and instruction. You are expected to infer a reasonable partitioning of the object into parts. Note that your partition should reflect common divisions of objects as they are understood in everyday life.

i.e. (human_body_part, object_body_part, edge_weight)

Each edge in this graph can take on a weight of 0, 1, 2, or 3, where:

- 0 indicates that the body part and object part connected by this edge remain relatively stationary with respect to each other over time.
- 1 indicates that the distance between the body part and the object part connected by this edge is steadily decreasing over time.
- 2 indicates that the distance between the body part and the object part connected by this edge is steadily increasing over time.
- 3 indicates that the relative movement trend between the human part and the object part is unstable or unclear over time.

Prompt section5: plan rules

1. All instructions pertain to the interaction task between a humanoid robot, modeled with relative simplicity and equipped with a ball rather than a finger on its hand, and an object. This interaction may be dynamic or static.

2. Each plan may involve sequential interactions with multiple objects. For each object, you should design a plan comprising at least five steps, including approaching and departing from the object.

3. Your return about relative_movement_dynamics should be formatted into sequence of $[(\text{human_body_part}, \text{object_body_part}, \text{edge_weight}), (\text{human_body_part}, \text{object_body_part}, \text{edge_weight}), \dots, 15 \text{ edges for one sequence.}]$

4. If you are confused about which part of the object you should select, you can select the root to represent the whole.

5. Be relatively sensitive to the judgment of relative movement dynamics, if it is not stable (e.g. when holding a box and walking towards destination, the feet and the box will alternately approach and move away from each other for a period of time), just set the weight to 3.

6. Your thought process may unfold as follows: perceive the surrounding scene context and identify the relevant object, decompose the instruction into a sequence of human-object interactions, imagine the corresponding motions, and represent each sub-sequence in the form of RMD.

Figure 5: Details of prompt section.

864
865
866
867
868
869
870
871
872
873
874
875
876
877
878
879
880
881
882
883
884
885
886
887
888
889
890
891
892
893
894
895
896
897
898
899
900
901
902
903
904
905
906
907
908
909
910
911
912
913
914
915
916
917

Prompt section6: reference example

Instruction: Take away clothes and have a rest.

Top-view image:

step1: get close to the laundry basket.

{
 human_root_target: laundry basket(back),
 object_root_target: laundry basket(center),
 relative_movement_dynamics:

[
 ("pelvis", "root", "1"),
 ("torso", "root", "1"),
 ("head", "root", "1"),
 ("left_upper_arm", "basket_left_side", "1"),
 ("left_lower_arm", "basket_left_side", "1"),
 ("left_hand", "basket_left_side", "1"),
 ("right_upper_arm", "basket_right_side", "1"),
 ("right_lower_arm", "basket_right_side", "1"),
 ("right_hand", "basket_right_side", "1"),
 ("left_thigh", "root", "3"),
 ("left_shin", "root", "3"),
 ("left_foot", "root", "3"),
 ("right_thigh", "root", "3"),
 ("right_shin", "root", "3"),
 ("right_foot", "root", "3")
]
}

Prompt section6: reference example

step2: bends down to grab the box with both hands and picks it up.

{
 human_root_target: laundry basket(back),
 object_root_target: laundry basket(center),
 relative_movement_dynamics:
 [
 ("pelvis", "root", "1"),
 ("torso", "root", "1"),
 ("head", "root", "1"),
 ("left_upper_arm", "basket_left_side", "0"),
 ("left_lower_arm", "basket_left_side", "0"),
 ("left_hand", "basket_left_side", "0"),
 ("right_upper_arm", "basket_right_side", "0"),
 ("right_lower_arm", "basket_right_side", "0"),
 ("right_hand", "basket_right_side", "0"),
 ("left_thigh", "root", "3"),
 ("left_shin", "basket_left_side", "2"),
 ("left_foot", "basket_left_side", "2"),
 ("right_thigh", "root", "3"),
 ("right_shin", "basket_right_side", "2"),
 ("right_foot", "basket_right_side", "2")
]
}

step3: walking to the washing machine while holding the laundry basket.

{
 human_root_target: washing machine(front),
 object_root_target: washing machine(front),
 relative_movement_dynamics:
 [
 ("pelvis", "root", "0"),
 ("torso", "root", "0"),
 ("head", "root", "0"),
 ("left_upper_arm", "basket_left_side", "0"),
 ("left_lower_arm", "basket_left_side", "0"),
 ("left_hand", "basket_left_side", "0"),
 ("right_upper_arm", "basket_right_side", "0"),
 ("right_lower_arm", "basket_right_side", "0"),
 ("right_hand", "basket_right_side", "0"),
 ("left_thigh", "root", "3"),
 ("left_shin", "root", "3"),
 ("left_foot", "root", "3"),
 ("right_thigh", "root", "3"),
 ("right_shin", "root", "3"),
 ("right_foot", "root", "3")
]
}

Prompt section6: reference example

step4: put down the laundry basket.

{
 human_root_target: washing machine(front),
 object_root_target: washing machine(front),
 relative_movement_dynamics:
 [
 ("pelvis", "root", "2"),
 ("torso", "root", "2"),
 ("head", "root", "2"),
 ("left_upper_arm", "basket_left_side", "0"),
 ("left_lower_arm", "basket_left_side", "0"),
 ("left_hand", "basket_left_side", "0"),
 ("right_upper_arm", "basket_right_side", "0"),
 ("right_lower_arm", "basket_right_side", "0"),
 ("right_hand", "basket_right_side", "0"),
 ("left_thigh", "root", "3"),
 ("left_shin", "basket_left_side", "1"),
 ("left_foot", "basket_left_side", "1"),
 ("right_thigh", "root", "3"),
 ("right_shin", "basket_right_side", "1"),
 ("right_foot", "basket_right_side", "1")
]
}

step5: get close to the chair.

{
 human_root_target: chair(front),
 object_root_target: chair(center),
 relative_movement_dynamics:
 [
 ("pelvis", "root", "1"),
 ("torso", "root", "1"),
 ("head", "root", "1"),
 ("left_upper_arm", "root", "1"),
 ("left_lower_arm", "root", "1"),
 ("left_hand", "root", "1"),
 ("right_upper_arm", "root", "1"),
 ("right_lower_arm", "root", "1"),
 ("right_hand", "root", "1"),
 ("left_thigh", "root", "3"),
 ("left_shin", "root", "3"),
 ("left_foot", "root", "3"),
 ("right_thigh", "root", "3"),
 ("right_shin", "root", "3"),
 ("right_foot", "root", "3")
]
}

Prompt section6: reference example

step6: sit down.

{
 human_root_target: chair(center),
 object_root_target: chair(center),
 relative_movement_dynamics:
 [
 ("pelvis", "seat_support", "1"),
 ("torso", "root", "3"),
 ("head", "root", "3"),
 ("left_upper_arm", "root", "3"),
 ("left_lower_arm", "root", "3"),
 ("left_hand", "root", "3"),
 ("right_upper_arm", "root", "3"),
 ("right_lower_arm", "root", "3"),
 ("right_hand", "root", "3"),
 ("left_thigh", "chair_foot", "0"),
 ("left_shin", "chair_foot", "0"),
 ("left_foot", "chair_foot", "0"),
 ("right_thigh", "chair_foot", "0"),
 ("right_shin", "chair_foot", "0"),
 ("right_foot", "chair_foot", "0")
]
}

step7: have a rest.

{
 human_root_target: chair(center),
 object_root_target: chair(center),
 relative_movement_dynamics:
 [
 ("pelvis", "seat_support", "0"),
 ("torso", "back_soft_support", "1"),
 ("head", "head_pillow", "1"),
 ("left_upper_arm", "root", "3"),
 ("left_lower_arm", "left_arm_sofa", "1"),
 ("left_hand", "root", "3"),
 ("right_upper_arm", "root", "3"),
 ("right_lower_arm", "right_arm_sofa", "1"),
 ("right_hand", "root", "3"),
 ("left_thigh", "chair_foot", "0"),
 ("left_shin", "chair_foot", "0"),
 ("left_foot", "chair_foot", "0"),
 ("right_thigh", "chair_foot", "0"),
 ("right_shin", "chair_foot", "0"),
 ("right_foot", "chair_foot", "0")
]
}

Figure 6: Details of prompt section

918 These relative positions are defined with respect to a local coordinate system centered on the refer-
 919 ence object.
 920

921 **RMD Concept Definition.** This section of the prompt helps the planner understand the concept of
 922 RMD, clarifies its intended semantics, introduces a method for instantiating it, and provides a formal
 923 definition of its instantiated form.
 924

925 **Specific Plan Instance.** This section presents a templated instance of an RMD-based plan, illus-
 926 trating the correspondence between the template elements and RMD components, as well as how
 927 such an instance aligns with a real-world interaction scenario. This helps the planner internalize the
 928 concept and encourages outputs that conform to the desired format.
 929

930 **Idea Outline.** This section offers a high-level overview of our approach, specifying the expected
 931 input and output of the interaction planner. Human–object interaction tasks are decomposed into a
 932 sequence of sub-steps, each characterized by consistent movement dynamics.
 933

934 **Plan Rules.** This section enumerates the rules that the planner must follow, emphasizing their signif-
 935 icance in prompt engineering. These rules define task interaction boundaries, output formatting, and
 936 criteria for determining movement dynamics. By adhering to these rules, the planner can effectively
 937 decompose complex interactions into manageable and coherent sub-sequences.
 938

939 **Reference Example.** Empirical findings from the NLP community indicate that one-shot prompt-
 940 ing often yields significantly better results than zero-shot prompting. Guided by this insight, we
 941 include a complete input–output example in the prompt to help the planner better understand the
 942 task expectations and output format.
 943

944 B INTERPLAY DATASET

945 To evaluate our framework in long-horizon, multi-task scenarios, we construct a novel dataset, *Inter-
 946 Play*, which encompasses both static and dynamic interaction tasks under diverse indoor scene
 947 contexts. Each data sample includes: (i) a list of processed 3D assets ready for direct use in sim-
 948 ulation, (ii) the corresponding 3D scene layout, (iii) a top-view rendered image, and (iv) a natural
 949 language instruction describing the intended task.
 950

951 In building the *InterPlay* dataset, we incorporate high-quality 3D object assets from several existing
 952 datasets, including PartNet (Mo et al., 2019), 3D-FRONT (Fu et al., 2021), SAMP (Hassan
 953 et al., 2021), CIRCLE (Araújo et al., 2023), and PartNet-Mobility (Xiang et al., 2020). From these
 954 sources, we carefully select 117 assets spanning categories such as bed, chair, sofa, washing
 955 machine, box, door, window, and wardrobe. Each asset is normalized, segmented into functional parts,
 956 and associated with part-level point clouds, based either on existing annotations or manual labeling.
 957

958 To generate scene layouts, we apply a set of heuristic rules that ensure: (i) a well-distributed ar-
 959 rangement without object collisions, (ii) semantically meaningful placements aligned with typical
 960 household settings, and (iii) a minimum of two interactive objects and at least two furniture items per
 961 scene, thereby enriching the contextual complexity of human–object interaction. We then populate
 962 these layout templates by randomly sampling from the processed asset pool.
 963

964 For each completed layout, we render a top-view image and employ GPT-4V Achiam et al. (2023)
 965 to generate a corresponding task instruction grounded in the scene context. Finally, we apply our
 966 VLM-guided RMD Planner to produce interaction plans, which are manually reviewed and refined
 967 before inclusion in the dataset.
 968

969 In total, *InterPlay* contains 1,210 interaction plans, covering a wide range of HOI behaviors involv-
 970 ing static, dynamic, and articulated objects with varying temporal lengths, all situated in realistic,
 971 household-inspired environments.
 972

973 C ADDITIONAL DETAILS OF REINFORCEMENT LEARNING

974 Our physics-based animation framework is built upon goal-conditioned reinforcement learning. At
 975 each time step t , the agent samples an action from its policy $\pi(a_t | s_t, g_t)$ based on the current state
 976 s_t and the goal state g_t . After executing the action, the environment transitions to the next state
 977 s_{t+1} , and the agent receives a task reward $r^G(s_t, g_t, s_{t+1})$. Further details are provided below.
 978

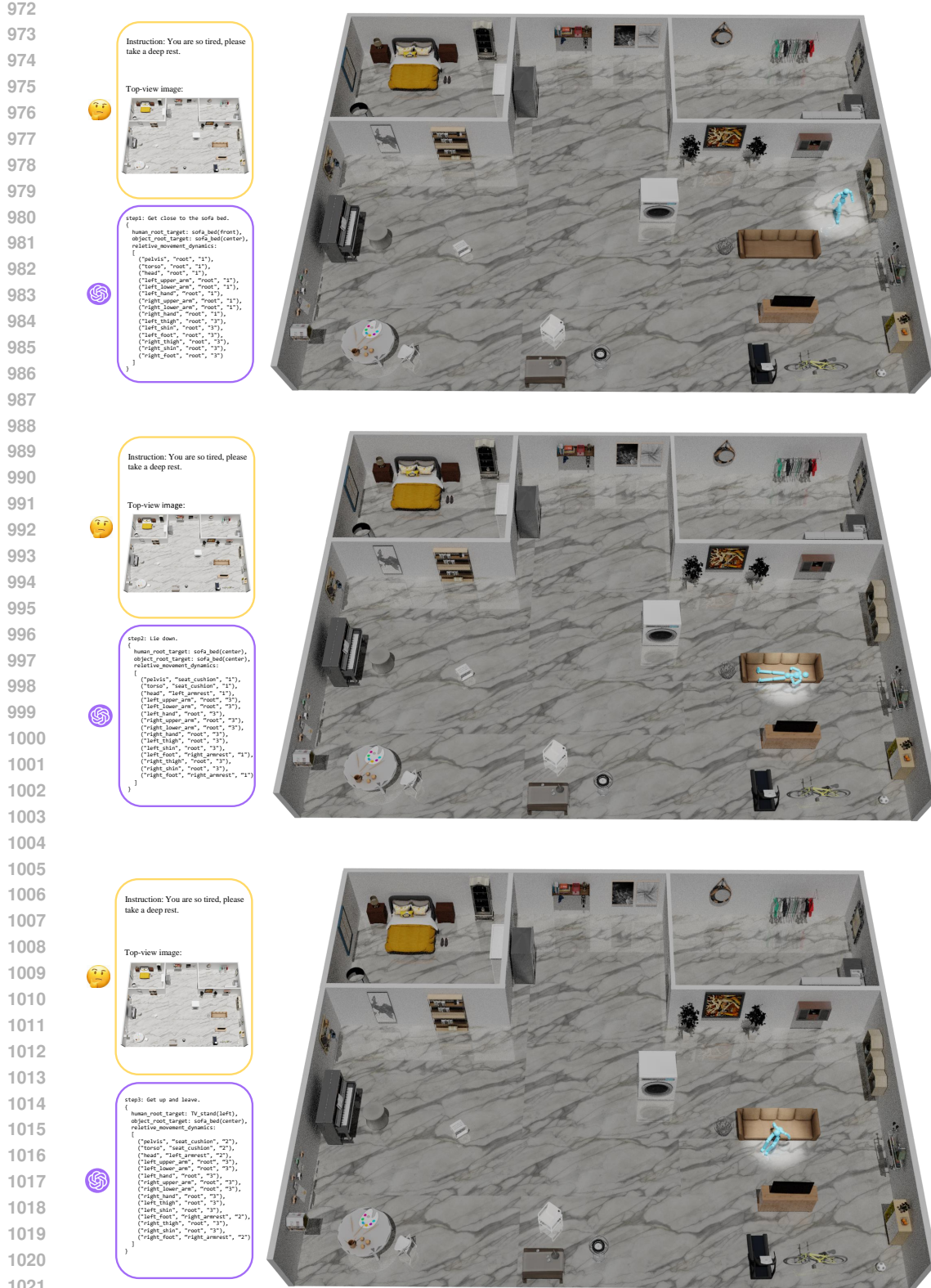


Figure 7: Visualization of long-term interaction with objects in an indoor home setting (part 1).

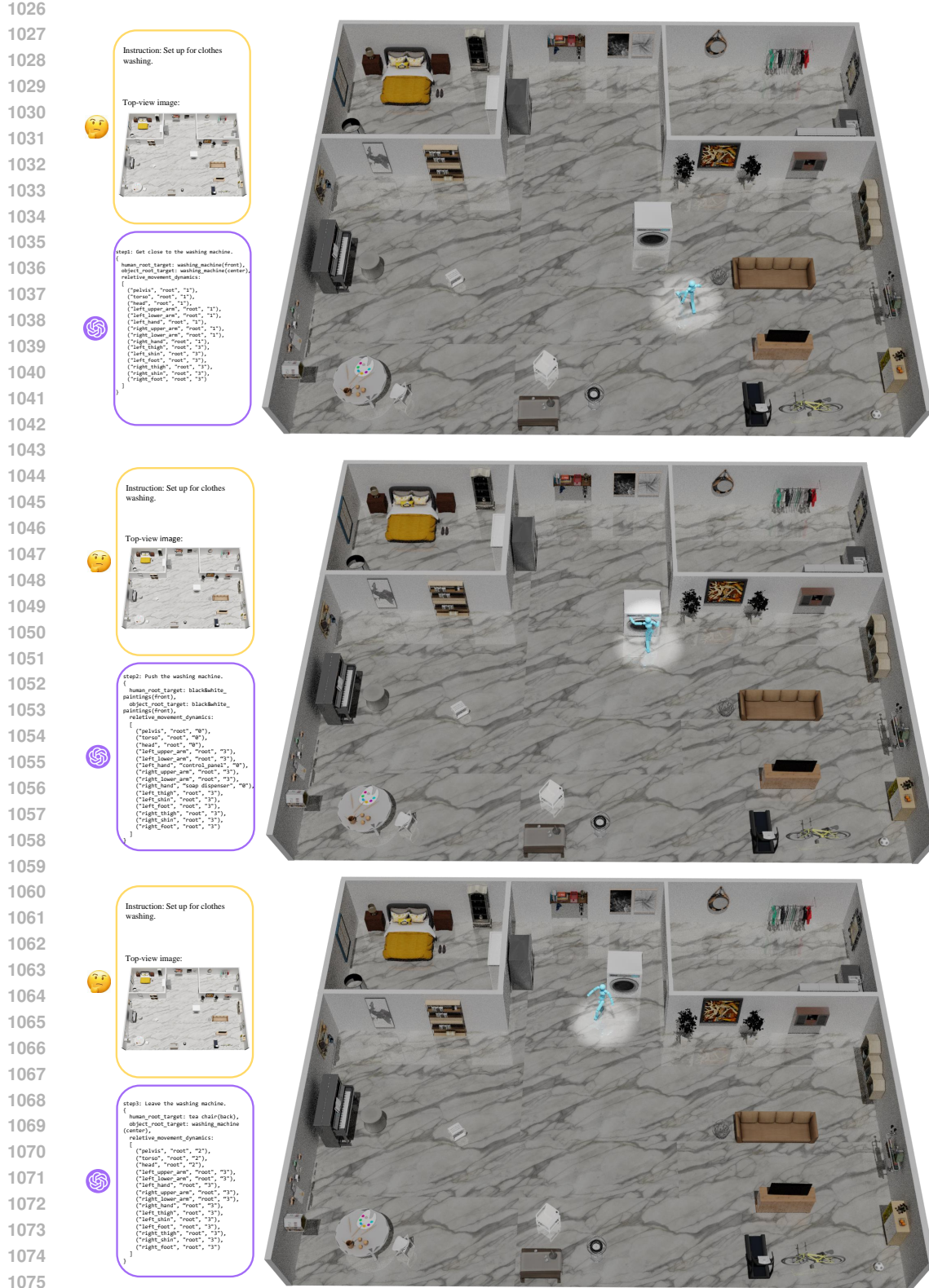


Figure 8: Visualization of long-term interaction with objects in an indoor home setting (part 2).

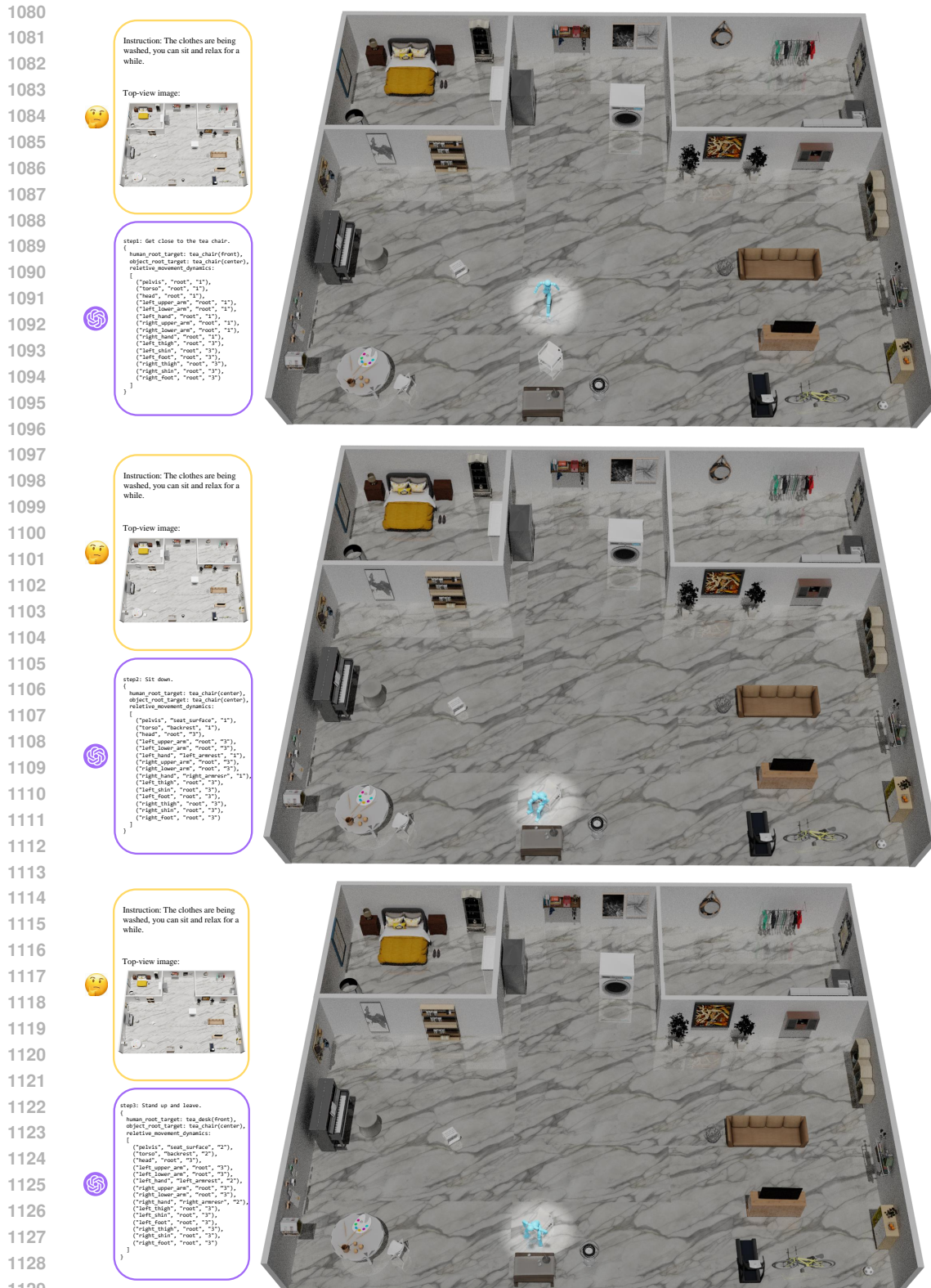


Figure 9: Visualization of long-term interaction with objects in an indoor home setting (part 3).

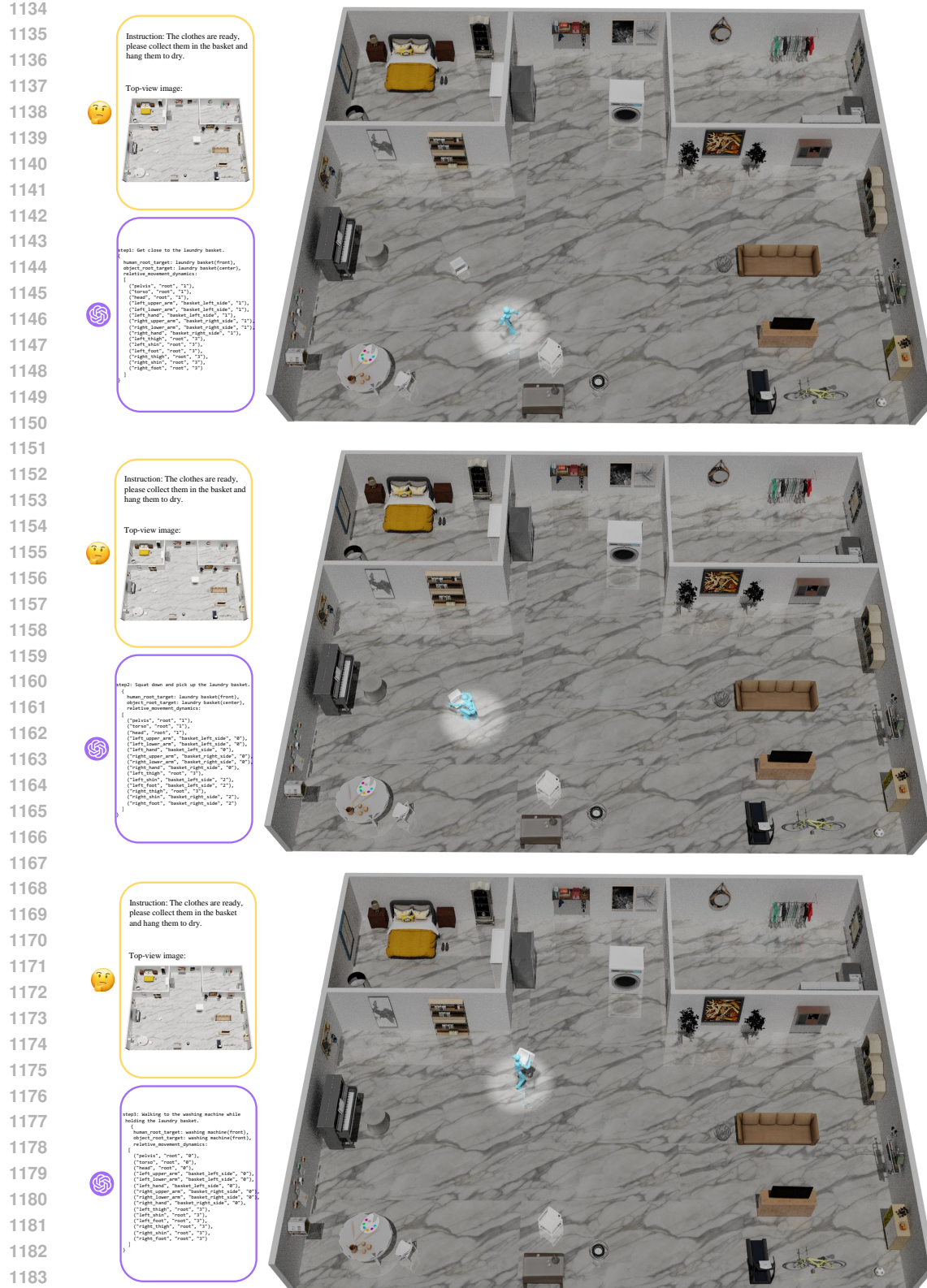


Figure 10: Visualization of long-term interaction with objects in an indoor home setting (part 4).

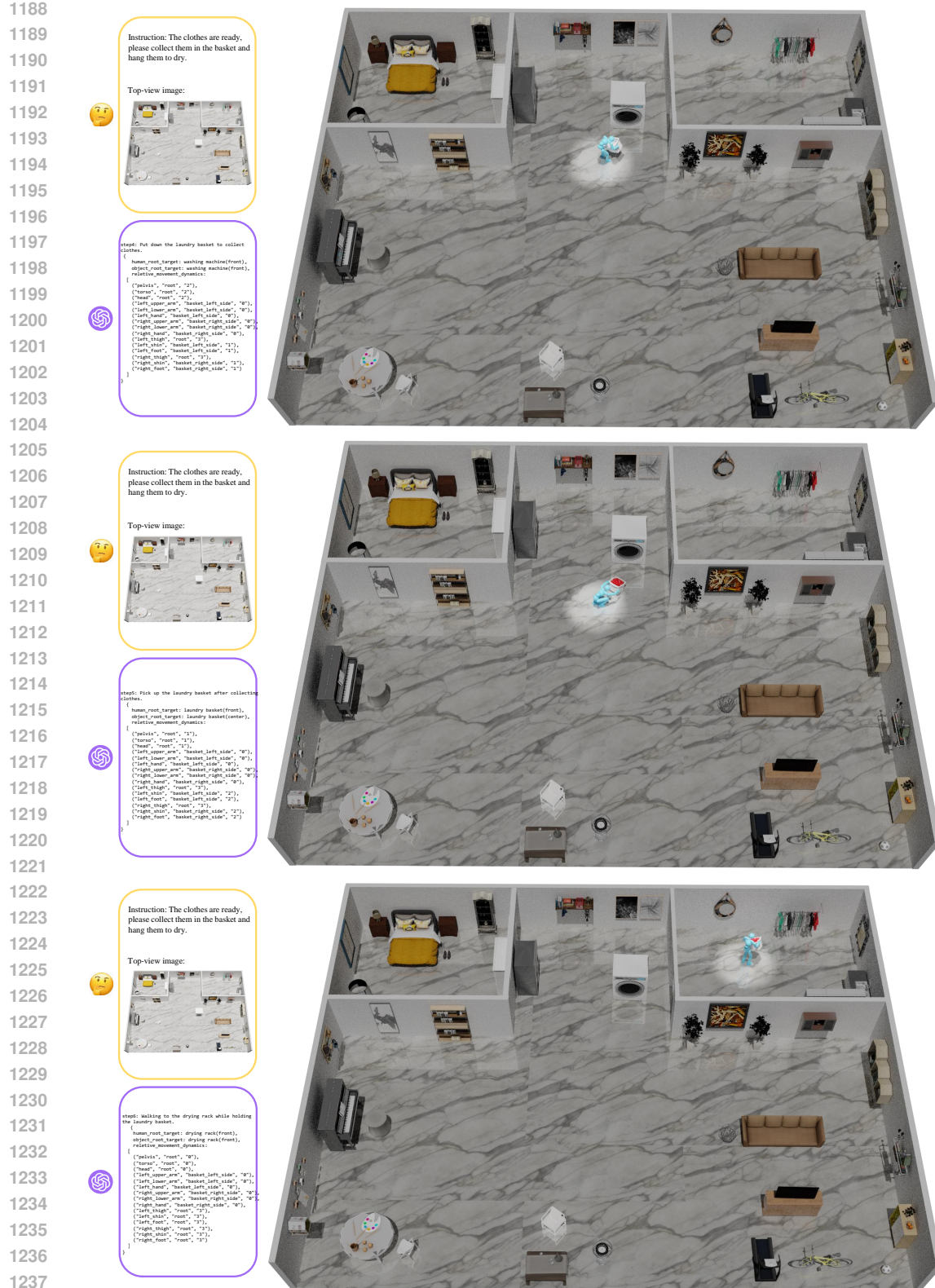


Figure 11: Visualization of long-term interaction with objects in an indoor home setting (part 5).

Action. We use a simulated humanoid character with 28 degrees of freedom (DoF), represented as a kinematic structure composed of 15 rigid bodies. The action space is defined as the target joint positions for 28 proportional-derivative (PD) controllers. At each timestep, the predicted actions specify these targets, which are then translated by the PD controllers into joint torques to drive the character’s motion.

Proprioception. The proprioceptive state \mathbf{s}_t is a 223-dimensional feature vector that encodes the character’s physical state. It includes the positions, rotations, linear velocities, and angular velocities of all rigid bodies, expressed in the character’s local coordinate frame. The only exception is the root height, which is represented in the world coordinate frame to preserve global elevation information.

Task Reward. Recall that the term r_{RMD} encourages each edge $e_{ij} \in \mathcal{B}$, representing a (*human-part, object-part*) pair, to follow the relative motion dynamics specified by its associated edge weight w_{ij} , as planned by the VLM. Specifically, r_{RMD} is computed by summing the individual alignment reward $r_{\text{rmd}}^{ij}(\cdot)$, each of which measures how well the pair (p_{hi}, p_{oj}) follows the motion pattern defined by w_{ij} , weighted by a coefficient λ_{ij} ,

$$r_{\text{RMD}} = \sum_{(i,j) \in E} \lambda_{ij} \cdot r_{\text{rmd}}(\tilde{\mathbf{p}}_{ij}, \tilde{\mathbf{v}}_{ij}, w_{ij}). \quad (15)$$

Specifically, we formally define $r_{\text{rmd}}(\tilde{\mathbf{p}}_{ij}, \tilde{\mathbf{v}}_{ij}, w_{ij})$ as,

$$r_{\text{rmd}}(\tilde{\mathbf{p}}_{ij}, \tilde{\mathbf{v}}_{ij}, w_{ij}) = \begin{cases} \exp\left(-(\tilde{\mathbf{p}}_{ij} \cdot \tilde{\mathbf{v}}_{ij})^2\right), & w_{ij} = 0, \\ \frac{1}{2} \exp\left(-\|\tilde{\mathbf{p}}_{ij}\|_2^2\right) + \frac{1}{2} \exp\left(-\left(\tilde{\mathbf{v}}_{ij} \cdot \frac{\tilde{\mathbf{p}}_{ij}}{\|\tilde{\mathbf{p}}_{ij}\|_2} + v^*\right)^2\right), & w_{ij} = 1, \\ \frac{1}{2} \left(1 - \exp\left(-\|\tilde{\mathbf{p}}_{ij}\|_2^2\right)\right) + \frac{1}{2} \exp\left(-\left(\tilde{\mathbf{v}}_{ij} \cdot \frac{\tilde{\mathbf{p}}_{ij}}{\|\tilde{\mathbf{p}}_{ij}\|_2} - v^*\right)^2\right), & w_{ij} = 2, \\ 1, & w_{ij} = 3. \end{cases} \quad (16)$$

The behavior of each reward term varies depending on the value of w_{ij} :

- When $w_{ij} = 0$, the reward promotes either a vanishing relative velocity or an orthogonal orientation between the relative position and velocity, thereby minimizing directional alignment.
- For $w_{ij} = 1$, the goal is to maintain spatial proximity while aligning the relative velocity with the direction of the relative position. In particular, the velocity projection is encouraged to approach a predefined target $v^* = 1$ m/s.
- When $w_{ij} = 2$, the reward favors increasing separation between parts, while ensuring that the leaving speed along the direction of displacement remains close to v^* .
- Finally, $w_{ij} = 3$ denotes an unstable or unpredictable relative motion trend. Here, the reward is set to a neutral constant value of 1 to avoid imposing misleading gradients.

Training details in a single-task scenario. Our policy network is divided into a critic network and an actor network, each starting with three multilayer perceptron (MLP) layers configured with [1024, 1024, 512] units. The discriminator network follows a similar architecture, also consisting of three MLP layers with [1024, 1024, 512] units. The hyperparameters used during the training process are detailed Tab. 4. Some baseline methods either did not implement certain HOI tasks (e.g., *open*, *push*) or failed to account for post-interaction transitions with static objects (e.g., *sit*, *lie*). To enable a fair and thorough comparison, we re-implemented these baselines with carefully hand-crafted goal states and reward functions for each task. This ensures that we can comprehensively evaluate the full interaction cycle: approaching the object, interacting with it, and departing afterward, across a range of individual HOI tasks. All methods were trained using a shared set of hyperparameters to maintain consistency.

Training details in a long-horizon multi-task scenario. Our policy consists of separate actor and critic networks, each implemented as a three-layer multilayer perceptron (MLP) with hidden dimensions of [1024, 1024, 512]. The discriminator network adopts the same architecture. Both our method and the baselines are trained using a two-stage procedure:

1296

1297

Table 4: Hyperparameters for RMD.

1298

1299

Hyperparameter	Value	Hyperparameter	Value	Hyperparameter	Value
Num. envs	4096	Max episode length	450	Num. epochs	25,000
Discount factor γ	0.99	GAE parameter λ	0.95	Minibatch size	16384
Optimizer	Adam	Learning rate	2e-5	Gradient clip norm	1.0
PPO horizon length	32	PPO clip ϵ	0.2	PPO miniepochs	6
Actor loss weight	1	Critic loss weight	5	Discriminator loss weight	5
AMP batch size	512	AMP sequence length t^*	10	AMP grad. penalty w^{gp}	5
Task reward weight α_{task}	0.5	Style reward weight α_{style}	0.5	Bounds loss coefficient	10

1300

1301

1302

1303

1304

1305

1306

(i) *Single-task pre-training*. We divide the parallel simulation environments into distinct subsets according to task type and difficulty, allowing the agent to learn basic interaction skills in a focused manner.

1307

1308

1309

(ii) *Long-horizon multi-task post-training*. For each environment instance, tasks are randomly sampled from our *InterPlay* dataset, promoting the agent’s ability to handle long-horizon human–object interaction tasks in complex and diverse scenes.

1310

1311

1312

To extend *InterPhys* to a multi-task setup, we concatenate all possible goal states and use a one-hot encoding to indicate the task identity. Additionally, we implement a script to translate the sequential plans in our dataset into the format required by other baselines (i.e., sequential goal states), thereby unifying the training pipeline. During execution, a rule-based finite-state machine is used to manage task transitions in both *InterPhys* and *TokenHSI*.

1313

1314

1315

1316

1317

D VISUALIZATIONS IN SUPPLEMENTARY MATERIAL

1318

1319

1320

1321

To complement the qualitative results presented in the main paper, we provide a demonstration video that combines the key aspects of our method. This video offers detailed visualizations showcasing the effectiveness of our framework in various real-world scenarios and compares it with competing approaches. It includes an overview of the motivation, challenges, main pipeline, and both quantitative and qualitative results. Additionally, the video highlights long-horizon interactions in both single-task and multi-task scenarios, involving static, dynamic, and articulated objects within a realistic indoor setting. In the single-task scenario, we present a comparison of our method with UniHSI (Xiao et al., 2024) for the sitting task and InterPhys (Hassan et al., 2023) for the door-opening task. While UniHSI struggles with high-frequency jitter and unrealistic motion, our method ensures smooth, human-like transitions. Similarly, in the door-opening task, our approach uses coordinated hand movements for a more lifelike interaction, in contrast to InterPhys, which relies solely on body movement and produces unnatural results. The multi-task scenario illustrates how our method excels by leveraging human-like motion, a unified objective design across different tasks, and the capabilities of Vision-Language Models to generate contextually relevant action plans. Additionally, we provide detailed visualizations alongside the Planner’s output, as shown in Fig. 7, Fig. 8, Fig. 9, Fig. 10 and Fig. 11.

1337

1338

E ABLATION STUDY ON THE VLM PLANNER

1339

1340

1341

1342

1343

1344

1345

Model and prompt variants. To assess the robustness of our approach, we performed ablation experiments by (i) replacing GPT-4V with other models such as LLaVA-1.6 and Qwen-VL-Max, and (ii) simplifying the prompt. As shown in Tab. 5, our framework remains effective across different VLMs and prompt designs, with only moderate performance differences. This is possible because our framework is modular, and the VLM planner functions as a plug-in component that can be replaced by any vision-language model with basic visual understanding and reasoning capabilities.

1346

1347

1348

1349

Planner label accuracy on InterPlay. To further quantify planner reliability, we manually annotated ideal RMD labels for key human-object pairs across all tasks in each subset (static, dynamic, and hybrid) and compared them with the planner’s outputs. The empirical rate of contradictory labels is 8.9%, 11.2%, and 14.7% for static, dynamic, and hybrid tasks, respectively, with higher error

1350

1351 Table 5: Comparison of VLM choice and prompt designs.

VLM	Completion Rate (%) \uparrow	Sub-step Completion Ratio (%) \uparrow	Sub-step Precision (cm) \downarrow
LLaVA-1.6	43.3	67.8	13.1
Qwen-VL-Max	47.7	68.3	12.7
GPT-4V (Simplified Prompt)	45.3	66.1	12.9
GPT-4V	53.8	71.8	11.2

1356

1357 on hybrid tasks due to their complex multi-stage nature. Together with the ablations in Tab. 5, this
 1359 analysis indicates that our framework is robust to moderate planner imperfections.

1360

1361 **Part decomposition on novel objects.** To further evaluate the planner’s behavior on unseen assets,
 1362 we additionally construct 100 new HOI tasks involving 50 objects that do not appear in the InterPlay
 1363 dataset and manually inspect the VLM planner’s part decompositions. Only 7 out of 100 cases
 1364 exhibit clearly unreasonable part splits, suggesting that the planner generalizes reasonably well to
 1365 unfamiliar but semantically common objects, likely due to its web-scale pretraining.

1366

1367 **Stage-transition threshold.** To evaluate the sensitivity of our method to the stage-transition
 1368 threshold, we perform an ablation study on the InterPlay-Hybrid subset by sweeping the thresh-
 1369 old from 0.80 to 0.95. As shown in Tab. 6, performance varies smoothly between 0.80 and 0.90
 1370 and peaks at 0.90, while only the extreme setting 0.95 leads to a clear drop in completion and pre-
 1371 cision. Based on these results, we keep 0.90 as the default threshold, since it offers the best trade-off
 1372 between completion, sub-step ratio, and precision while the range [0.80, 0.90] is generally stable.

1373

1374

1375 Table 6: Comparison of threshold choice.

Threshold	Completion Rate (%) \uparrow	Sub-step Completion Ratio (%) \uparrow	Sub-step Precision (cm) \downarrow
0.80	47.9	65.6	13.5
0.85	51.0	67.2	12.9
0.90	53.8	71.8	11.2
0.95	32.8	47.2	16.7

1379

1382 F USER STUDY

1383

1384 To evaluate the visual quality and goal alignment of the generated motions from a human-centric
 1385 perspective, we conducted a user study with 20 participants. Each participant watched 20 motion se-
 1386 quences, each paired with its corresponding task description, and rated them on two criteria: Motion
 1387 Realism (assessing whether the interaction appears natural and physically plausible) and Task Con-
 1388 sistency (measuring how well the motion aligns with the task objective). Each criterion was rated
 1389 on a scale from 0 to 5, where higher scores indicate better performance. The results, summarized in
 1390 Tab. 7, show that our method achieves superior performance in both realism and task alignment.

1391

1392

1393 Table 7: Comparison of motion realism and task consistency.

Method	Motion Realism \uparrow	Task Consistency \uparrow
InterPhys	3.2 ± 0.7	3.5 ± 0.5
TokenHSI	3.4 ± 0.4	3.7 ± 0.6
UniHSI	3.1 ± 0.5	3.7 ± 0.4
Ours	4.0 ± 0.4	4.1 ± 0.3

1398

1399

1400

1401 G LIMITATIONS AND FUTURE WORK

1402

1403

Limitations. While our framework advances dynamic human-object interaction modeling, it cur-
 1403 rently focuses on single-agent scenarios and does not address multi-agent interactions (e.g. col-

1404
 1405 laborative tasks involving multiple humans or agents) or social dynamics (e.g. social impact con-
 1406 siderations in shared environments). This restricts its applicability to real-world settings requiring
 1407 coordination among multiple agents, such as collaborative kitchens or assistive care scenarios. Ad-
 1408 ditionally, the current VLM-based planner may struggle with long-horizon tasks that demand ex-
 1409 tended temporal reasoning and hierarchical planning. For instance, tasks like cooking multi-step
 1410 meals or tidying interconnected household spaces remain challenging due to the lack of explicit task
 1411 decomposition mechanisms.

1412 **Future Work.** To address these gaps, future research directions include extending the framework to
 1413 multi-agent reinforcement learning, where agents could learn adaptive communication protocols and
 1414 dynamic role allocation in socially rich environments. Simultaneously, integrating chain-of-thought
 1415 prompting into the VLM-based planner could enhance its capacity for stepwise task decompositon
 1416 (e.g., sequencing ingredient preparation, cooking, and serving), improving robustness in household
 1417 robotics scenarios. Combining multi-agent social coordination and hierarchical reasoning would
 1418 bridge the gap between atomic interactions and goal-oriented task execution, enabling scalable de-
 1419 ployment in collaborative human environments.

1420 H STATEMENTS

1421
 1422 **Ethics Statement.** This work complies with the ICLR Code of Ethics. The research involves no
 1423 human subjects or sensitive personal data. All datasets are publicly available, and their use strictly
 1424 follows the corresponding licenses and established ethical standards.

1425
 1426 **Reproducibility Statement.** This work complies with the ICLR standards of reproducibility. We
 1427 provide detailed descriptions of the experimental settings, model configurations, and evaluation pro-
 1428 tocols in the main text and appendix, ensuring that our results can be independently verified.

1429
 1430 **LLM Usage Statement.** We disclose that large language models (LLMs) were used solely for
 1431 grammar checking and minor text polishing. All aspects of the research design, experimentation,
 1432 analysis, and results remain entirely the responsibility of the authors.